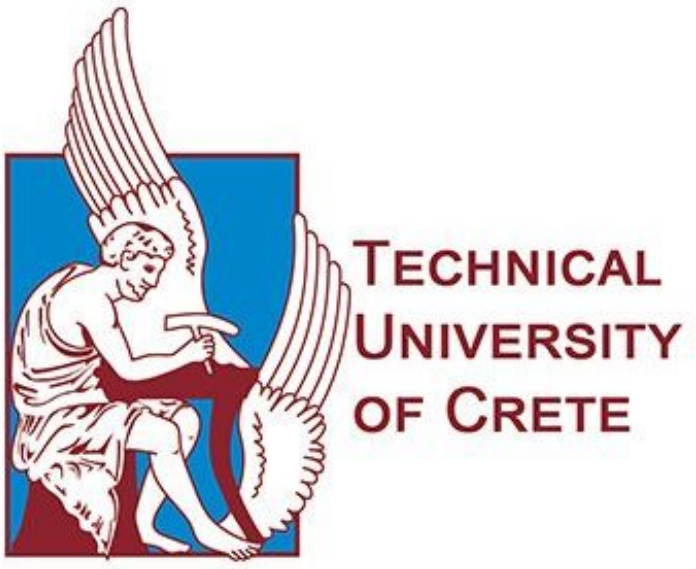

Blind FSK Detection in SIMO Systems

Submitted to the Department of Electrical and Computer Engineering in partial fulfillment of the requirements for the ECE Diploma Degree

By: Nikolaos Nasoulis

Advisor: Professor George Karystinos

Committee Member: Professor Aggelos Bletsas

Committee Member: Professor Athanasios Liavas

Department of Electrical and Computer Engineering

Technical University of Crete

Greece

2022

Abstract

Noncoherent (blind) sequence detection offers significant performance gains in comparison with conventional single-symbol noncoherent detection when the communication channel is quasi-static, at the cost of increased (usually exponential in the sequence length) complexity. In 2015, optimal blind frequency-shift keying (FSK) sequence detection in single-input single-output (SISO) systems was proven to be polynomially solvable and quasilinear-complexity optimal detectors were developed. In this thesis, we examine the complexity of optimal blind FSK sequence detection in 1x2 single-input multiple-output (SIMO) systems, i.e., systems with one transmit and two receive antennas. We focus on the case of 3-FSK modulation, prove that optimal blind FSK sequence detection is polynomially solvable for these cases, and present an efficient detection algorithm that has worst-time complexity $O(N^3)$ where N is the sequence length. Finally, we offer a few insights on generalizing these results for higher-order FSK modulation and larger number of receive antennas.

Contents

Chapter 1

Introduction

FSK (frequency-shift keying) is a type of orthogonal modulation which, like other types of orthogonal modulations, is typically preferred in relatively low-rate communication systems that operate in the power-limited regime. Specifically, FSK is primarily used, or considered for future use, in underwater communications [1, 2, 3, 4, 5, 6, 7], acoustic short-range communications [8, 9], power-line communications [10, 11], backscatter sensor networks and RFID [12, 13, 14, 15, 16], low-power wireless sensor networks [17], and cooperative communications [18, 19, 20, 21, 22, 23]. In order to avoid the need for channel estimation, which induces added complexity at the receiver end and rate loss due to the necessary use of a pilot sequence, systems that utilize orthogonal modulation usually operate in the noncoherent mode, i.e., the receiver performs noncoherent (or blind) detection without any channel knowledge [8, 10, 13, 18, 19, 20, 21, 23, 24, 25, 26, 27]. This is partly due to the simplicity of the single-symbol noncoherent detector which, for orthogonal modulation (e.g., FSK), is a simple energy detector [8, 18, 19, 20, 21, 25, 26, 27, 28].

Moreover, it has been shown in [29, 30] that noncoherent sequence detection can offer significant performance gains in comparison with conventional single-symbol noncoherent detection, as due to channel-induced memory, the optimal noncoherent detector requires processing of the

entire received sequence to make a decision on the entire data sequence, i.e., it is a sequence detector and no longer a single-symbol one. It was firstly demonstrated in [31, 32, 33, 34], in the context of M-ary PSK (MPSK), that the ML noncoherent sequence detection minimizes the sequence error probability, offering significant error rate performance gains over the conventional symbol-by-symbol noncoherent detection and attaining nearly-coherent detection performance for sufficiently long sequences.

Specifically for FSK modulation, noncoherent sequence detection has been considered in [10, 14, 23, 24, 35, 36], however optimal sequence detection can reach exponential (in the sequence length) complexity when implemented through an exhaustive search among all possible transmitted data sequences, as it was shown in [23, 35, 36]. Howbeit, by utilising principles that have been used for polynomial-complexity optimization in [37, 38, 39, 40], it was shown for the first time in [71], that GLRT-optimal noncoherent sequence detection of orthogonally modulated signals in flat fading is achievable with log-linear (in the sequence length) complexity.

In wireless communications, MIMO (Multiple-input Multiple-output) is a method for multiplying the capacity of a radio link using multiple transmission and receiving antennas to exploit multipath propagation. It specifically refers to a practical technique for sending and receiving more than one data signal simultaneously over the same radio channel by exploiting multipath propagation. Although this 'multipath' phenomena may be interesting, it is the use of orthogonal frequency division multiplexing to encode the channels that's responsible for the increase in data capacity. MIMO technology has been standardized for wireless LANs, 3G mobile phone networks, and 4G mobile phone networks and is currently in widespread commercial use. MIMO can be used in different format, depending on the number of the antennas used in the receiver and/or transmitter. This work addresses the use of SIMO (Single-input Mutiple-output), a specialised format of MIMO, where the transmitter has a single antenna and the receiver has multiple antennas. This is also known as receive diversity and it is often

used to enable a receiver system that receives signals from a number of independent sources to combat the effects of fading. It has been used for many years with short wave listening / receiving stations to combat the effects of ionospheric fading and interference.

In this work, we present an efficient algorithm that performs optimal noncoherent sequence detection of orthogonally modulated signals (presented in the context of FSK) in a SIMO Rayleigh fading channel. This work addresses the specialized case where the receiver utilises $D = 2$ antennas and $M = 3$ different symbol frequencies are transmitted (3FSK), but the algorithm can be generalized for any $D > 2$ and $M > 3$.

The rest of this work is organized as follows. In Chapter 2 the signal model is presented and the optimal FSK detector is determined firstly for symbol detection, building up to FSK sequence detection and FSK sequence detection in SIMO Rayleigh Fading channels. In Chapter 3 we introduce the concept of Spherical Coordinates and the efficient algorithm is presented and analysed, including both theoritical and algorithmic developments, as well as complexity analysis. Finally in Chapter 4, insights towards a $M > 3$ and $D > 2$ implementation are presented.

Chapter 2

Problem Statement

2.1 Signal Model & Optimal FSK Symbol Detection

M-ary FSK (MFSK) utilizes M sub-carrier frequencies to modulate the information symbol $x \in \mathcal{M} \triangleq \{1, 2, \ldots, M\}$. This means that we send through our transmitter the signal

$$\tilde{s}_x(t) = \sqrt{\frac{P}{T}} \cos 2\pi (F_c + F_x)t = \Re\{s_x(t) e^{j2\pi F_c t}\} \tag{2.1}$$

where

$$s_x(t) = \sqrt{\frac{P}{T}} e^{j2\pi F_x t}, \quad 0 \le t < T, \quad x \in \mathcal{M} \ , \tag{2.2}$$

and, after passing through the channel and L different paths, we have at our receiver

$$\tilde{r}(t) = \sum_{l=1}^{L} a_l \tilde{s}_x(t - \tau_l) + \tilde{n}(t) = \sum_{l=1}^{L} a_l \Re\{s_x(t - \tau_l) e^{j2\pi F_c (t - \tau_l)}\} + \Re\{n(t) e^{j2\pi F_c t}\} \tag{2.3}$$

where

$$\tilde{n}(t) = \Re\{n(t) e^{j2\pi F_c t}\} \ . \tag{2.4}$$

Considering $\tau_l \ll T_s$ for $l = 1, \ldots, L$, then $s(t - \tau_l) \to s(t)$ and we can write

$$\tilde{r}(t) = \sum_{l=1}^{L} \Re\{a_l e^{j2\pi F_c t} e^{-j2\pi F_c \tau_l} s_x(t)\} + \Re\{n(t) e^{j2\pi F_c t}\} = \Re\Big\{ e^{j2\pi F_c t} \Big(s_x(t) \sum_{l=1}^{L} a_l e^{-j2\pi F_c \tau_l} + n(t) \Big) \Big\}$$

$$= \Re\big\{ e^{j2\pi F_c t} \big(h s_x(t) + n(t) \big) \big\}$$

$$\Rightarrow \tilde{r}(t) = \Re\big\{e^{j2\pi F_c t} r(t)\big\} \tag{2.5}$$

where

$$r(t) = h s_x(t) + n(t) \tag{2.6}$$

and

$$h = \sum_{l=1}^{L} a_l e^{-j2\pi F_c \tau_l} \ . \tag{2.7}$$

The optimal receiver correlates the received signal $r(t)$ in (2.6) with all M signaling waveforms $s_1(t), s_2(t), \ldots, s_M(t)$ to produce the M samples

$$r_m = \frac{1}{\sqrt{P}} \int_0^T r(t) s_m^*(t)\, dt \quad m \in \mathcal{M} \ . \tag{2.8}$$

If the orthogonality condition is satisfied, i.e., $|F_m - F_{m'}| = k\frac{1}{2T}$, for some $k \in \mathbb{N}$, $\forall m, m' \in \mathcal{M}$ with $m \neq m'$, then

$$r_m = \begin{cases} \sqrt{P}h + n_m, & m = x, \\ n_m, & m \neq x, \end{cases} \tag{2.9}$$

where $n_1, n_2, \ldots, n_M \sim \mathcal{CN}(0, \sigma_n^2)$. Consequently, for a single-symbol duration, the received vector becomes

$$\underbrace{\begin{bmatrix} r_1 \\ \vdots \\ r_M \end{bmatrix}}_{\mathbf{r}} = \sqrt{P} h \mathbf{e}_x + \underbrace{\begin{bmatrix} n_1 \\ \vdots \\ n_M \end{bmatrix}}_{\mathbf{n}} \tag{2.10}$$

where $\mathbf{n} \sim \mathcal{CN}(\mathbf{0}, \sigma_n^2 \mathbf{I}_M)$ and $\mathbf{e}_x$ is the x-th column of the $M \times M$ identinty matrix $\mathbf{I}_M$ that corresponds to the corellating frequency F_x and the corresponding symbol $x \in \mathcal{M}$. For notation simplicity, we also define the set

$$\mathcal{I}_M \triangleq \{\mathbf{e}_1, \mathbf{e}_2, \ldots, \mathbf{e}_M\} \tag{2.11}$$

that consists of the M columns of $\mathbf{I}_M$.

We will consider two cases for any $M \in \mathbb{N}_{\geq 2}$, where h is either known or a random variable that follows the complex normal distribution with $h \sim \mathcal{CN}(0, \sigma_h^2)$. In both cases, if x is given, $\mathbf{r}$ is also complex normal distributed. Hence, the optimal receiver becomes

$$\boxed{\max_{x \in \mathcal{M}} f(\mathbf{r}|x) = \max_{x \in \mathcal{M}} \frac{1}{\pi^k |\mathbf{C}|} e^{-(\mathbf{r}-\boldsymbol{\mu})^H \mathbf{C}^{-1} (\mathbf{r}-\boldsymbol{\mu})}} \tag{2.12}$$

where $f(\mathbf{r}|x)$ stands for the pertinent PDF of $\mathbf{r}$ given x, $\boldsymbol{\mu}$ is the mean vector of $\mathbf{r}$ given x, and $\mathbf{C}$ is the covariance matrix of $\mathbf{r}$ given x. We study the two cases seperately.

1. h is known:

   Since h is known,

$$\boldsymbol{\mu} = \mathbb{E}[\mathbf{r}|x] = \mathbb{E}[\sqrt{P}h\mathbf{e}_x|x] + \mathbb{E}[\mathbf{n}|x] = \sqrt{P}h\mathbf{e}_x \tag{2.13}$$

   and

$$\mathbf{C} = \mathbb{E}[(\mathbf{r}-\boldsymbol{\mu})(\mathbf{r}-\boldsymbol{\mu})^H|x] = \mathbb{E}[\mathbf{n}\mathbf{n}^H|x] \Rightarrow \mathbf{C} = \sigma_n^2\mathbf{I}_M \ , \tag{2.14}$$

$$\mathbf{C}^{-1} = \frac{1}{\sigma_n^2}\mathbf{I}_M \ . \tag{2.15}$$

   As it is shown in Appendix A, the optimal decision is determined by

$$\boxed{\underset{x\in\mathcal{M}}{\operatorname{argmax}} f(\mathbf{r}|x) = \underset{x\in\mathcal{M}}{\operatorname{argmax}} \Re\{h^* r[x]\}} \ . \tag{2.16}$$

2. h is unknown and $h \sim \mathcal{CN}(0, \sigma_h^2)$:

   Since $h \sim \mathcal{N}(0, \sigma_h^2)$,

$$\boldsymbol{\mu} = \mathbb{E}[\mathbf{r}|x] = \mathbb{E}[\sqrt{P}h\mathbf{e}_x + \mathbf{n}|x] = \sqrt{P}\mathbb{E}[h|x]\mathbf{e}_x + \mathbb{E}[\mathbf{n}|x] = \mathbf{0} \tag{2.17}$$

   and it is shown in Appendix B that

$$|\mathbf{C}| = \sigma_n^{2M} + P\sigma_h^2\sigma_n^M \tag{2.18}$$

   and

$$\mathbf{C}^{-1} = \frac{1}{\sigma_n^2}\left(\mathbf{I}_M - \frac{P\sigma_h^2}{\sigma_n^2 + P\sigma_h^2}\mathbf{e}_x\mathbf{e}_x^H\right) \ . \tag{2.19}$$

   It is also shown in Appendix B that the optimal decision is determined by

$$\boxed{\underset{x\in\mathcal{M}}{\operatorname{argmax}} f(\mathbf{r}|x) = \underset{x\in\mathcal{M}}{\operatorname{argmax}} |r[x]|} \ . \tag{2.20}$$

2.2 Optimal FSK Sequence Detection

Considering the sequence $\mathbf{x} \triangleq (x_1, x_2, \ldots, x_N)$ of $N \in \mathbb{N}_{\geq 2}$ sent symbols, we have at our receiver

$$\underbrace{\begin{bmatrix} \mathbf{r}_1 \\ \vdots \\ \mathbf{r}_N \end{bmatrix}}_{\mathbf{y}} = \sqrt{P}h \underbrace{\begin{bmatrix} \mathbf{e}_{x_1} \\ \vdots \\ \mathbf{e}_{x_N} \end{bmatrix}}_{\mathbf{s}} + \mathbf{w} = \sqrt{P}h\mathbf{s} + \mathbf{w} \tag{2.21}$$

where $\mathbf{w} \sim \mathcal{CN}(\mathbf{0}, \sigma_w^2 \mathbf{I}_{MN})$ and $\mathbf{y}$, $\mathbf{s}$, and $\mathbf{w}$ are $MN \times 1$ vectors.

Equivalently with the single symbol case we want to maximize $f(\mathbf{y}|\mathbf{s})$ over $\mathbf{s} \in \mathcal{I}_M^N$ for both coherent and noncoherent detection, i.e.,

$$\boxed{\max_{\mathbf{s} \in \mathcal{I}_M^N} f(\mathbf{y}|\mathbf{s}) = \max_{\mathbf{s} \in \mathcal{I}_M^N} \frac{1}{\pi^k |\mathbf{C}|} e^{-(\mathbf{y}-\boldsymbol{\mu})^H \mathbf{C}^{-1} (\mathbf{y}-\boldsymbol{\mu})}} \tag{2.22}$$

where $\boldsymbol{\mu}$ is the mean vector of $\mathbf{y}$ given $\mathbf{s}$ and $\mathbf{C}$ is the covariance matrix of $\mathbf{y}$ given $\mathbf{s}$. We again study the two cases seperately.

1. h is known:

   As in the single symbol case, given the transmitted symbol sequence $\mathbf{s}$, the expected value of $\mathbf{y}$ is

   $$\boldsymbol{\mu} = \mathbb{E}[\mathbf{y}|\mathbf{s}] = \sqrt{P}h\mathbf{s} \tag{2.23}$$

   and its covariance matrix is

   $$\mathbf{C} = \mathbb{E}[(\mathbf{y} - \boldsymbol{\mu})(\mathbf{y} - \boldsymbol{\mu})^H |\mathbf{s}] = \mathbb{E}[\mathbf{w}\mathbf{w}^H] = \sigma_w^2 \mathbf{I}_{MN} \ . \tag{2.24}$$

   The inverse of the latter is

   $$\mathbf{C}^{-1} = \frac{1}{\sigma_w^2} \mathbf{I}_{MN}. \tag{2.25}$$

   As we can see in Appendix C, in this case the optimal desicion is determined by

   $$\boxed{\operatorname*{argmax}_{\mathbf{s} \in \mathcal{I}_M^N} f(\mathbf{y}|\mathbf{s}) = \operatorname*{argmax}_{\mathbf{s} \in \mathcal{I}_M^N} \Re\{h^* \mathbf{s}^T \mathbf{y}\} \equiv \operatorname*{argmax}_{\mathbf{x} \in \mathcal{M}^N} \sum_{n=1}^{N} \Re\{h^* y_n[x_n]\}} \ . \tag{2.26}$$

2. h is unknown and $h \sim \mathcal{CN}(0, \sigma_h^2)$:

Since $h \sim \mathcal{CN}(0, \sigma_h^2)$,

$$\boldsymbol{\mu} = \mathbb{E}[\mathbf{y}|\mathbf{s}] = \mathbb{E}[\sqrt{P}h\mathbf{s} + \mathbf{w}|\mathbf{s}] = \sqrt{P}\mathbb{E}[h|\mathbf{s}]\mathbf{s} + \mathbb{E}[\mathbf{w}|\mathbf{s}] = \mathbf{0} \tag{2.27}$$

and it is shown in Appendix D that

$$\mathbf{C} = P\mathbf{s}\mathbf{s}^H\sigma_h^2 + \sigma_w^2\mathbf{I}_{MN} \tag{2.28}$$

and

$$\mathbf{C}^{-1} = \frac{1}{\sigma_w^2}\left(\mathbf{I}_{MN} - \frac{P\sigma_h^2}{\sigma_w^2 + \sigma_h^2 NP}\mathbf{s}\mathbf{s}^H\right). \tag{2.29}$$

It is also shown in Appendix D that the optimal decision is determined by

$$\boxed{\underset{\mathbf{s}\in\mathcal{I}_M^N}{\operatorname{argmax}} f(\mathbf{y}|\mathbf{s}) = \underset{\mathbf{s}\in\mathcal{I}_M^N}{\operatorname{argmax}} |\mathbf{s}^T\mathbf{y}| \equiv \underset{\mathbf{x}\in\mathcal{M}^N}{\operatorname{argmax}} \left|\sum_{n=1}^{N} y_n[x_n]\right|}. \tag{2.30}$$

In [71], this problem was proven to be polynomically solvable and an optimal algorithm of complexity $O(N \log N)$ was provided.

2.3 Optimal FSK Sequence Detection in SIMO Rayleigh Fading

We consider the case of 1 transmit antenna and D receive antennas. The received data are stored in the $MN \times D$ matrix

$$\mathbf{Y}_{MN\times D} = \begin{bmatrix} h_1\mathbf{s}(1) & \dots & h_D\mathbf{s}(1) \\ \vdots & \ddots & \vdots \\ h_1\mathbf{s}(N) & \dots & h_D\mathbf{s}(N) \end{bmatrix} + \begin{bmatrix} \mathbf{n}_1(1) & \dots & \mathbf{n}_D(1) \\ \vdots & \ddots & \vdots \\ \mathbf{n}_1(N) & \dots & \mathbf{n}_D(N) \end{bmatrix} = \mathbf{s}\mathbf{h}^T + \mathbf{N} \tag{2.31}$$

where $M, N, D \in \mathbb{N}_{\geq 2}$, $\mathbf{s}(n) \in \mathcal{I}_M$, $\mathbf{n}_d(n) \sim \mathcal{CN}(\mathbf{0}, \sigma^2\mathbf{I}_M)$, $h_d \sim \mathcal{CN}(0, \sigma_h^2)$,
$\mathbf{h}_{D\times 1} = \begin{bmatrix} h_1 & h_2 & \dots & h_D \end{bmatrix}^T \sim \mathcal{CN}(\mathbf{0},\ \sigma_h^2\mathbf{I}_D)$, and $\mathbf{s}_{MN\times 1} = \begin{bmatrix} \mathbf{s}(1) & \mathbf{s}(2) & \dots & \mathbf{s}(N) \end{bmatrix}^T$.
Let $\mathbf{z} = \operatorname{vec}(\mathbf{Y})$. Then,

$$\mathbf{z} = \operatorname{vec}(\mathbf{Y}) = \operatorname{vec}(\mathbf{s}\mathbf{h}^T) + \operatorname{vec}(\mathbf{N}) = \mathbf{h} \otimes \mathbf{s} + \mathbf{w} \tag{2.32}$$

where $\mathbf{w}_{MND\times 1} = \text{vec}(\mathbf{N})$, $\mathbf{w} \sim \mathcal{CN}(\mathbf{0}, \sigma^2\mathbf{I}_{MND})$.

Also,

$$\boxed{f(\mathbf{Y}|\mathbf{s}) = f(\text{vec}(\mathbf{Y})|\mathbf{s}) = f(\mathbf{z}|\mathbf{s}) = \frac{1}{\pi^{MND}|\mathbf{C}|}e^{-(\mathbf{z}-\boldsymbol{\mu})^H\mathbf{C}^{-1}(\mathbf{z}-\boldsymbol{\mu})}} \tag{2.33}$$

where $\boldsymbol{\mu}$ is the mean vector of $\mathbf{z}$ given $\mathbf{s}$ and $\mathbf{C}$ is the covariance matrix of of $\mathbf{z}$ given $\mathbf{s}$. Again, we study the two cases for $\mathbf{h}$ separately.

1. $\mathbf{h}$ is known:

   Given the transmitted symbol sequence $\mathbf{s}$, the expected value of vector $\mathbf{z}$ is determined by

   $$\boldsymbol{\mu} = \mathbb{E}[\mathbf{z}|\mathbf{s}] = \mathbb{E}[\mathbf{h} \otimes \mathbf{s} + \mathbf{w}|\mathbf{s}] = \mathbf{h} \otimes \mathbf{s} \tag{2.34}$$

   and its covariance matrix by

   $$\mathbf{C} = \mathbb{E}[(\mathbf{z} - \boldsymbol{\mu})(\mathbf{z} - \boldsymbol{\mu})^H|\mathbf{s}] = \mathbb{E}[\mathbf{w}\mathbf{w}^H|\mathbf{s}] = \sigma^2\mathbf{I}_{MND} \ . \tag{2.35}$$

   We can see that the determinant $|\mathbf{C}|$ is the product of the diagonal units of $\mathbf{C}$ and is independent of $\mathbf{s}$. By maximizing and substituting in (2.33), we can see in Appendix E that the optimal decision is determined by

   $$\boxed{\underset{\mathbf{s}\in\mathcal{I}_M^N}{\text{argmax}}\, f(\mathbf{Y}|\mathbf{s}) = \underset{\mathbf{s}\in\mathcal{I}_M^N}{\text{argmax}}\, \Re\{\mathbf{s}^H\mathbf{Y}\mathbf{h}^*\} \equiv \underset{\mathbf{x}\in\mathcal{M}^N}{\text{argmax}} \sum_{n=1}^{N} \Re\{\mathbf{Y}_{n,:}[x_n]\mathbf{h}^*\}} \ . \tag{2.36}$$

2. $\mathbf{h}$ is unknown and $\mathbf{h} \sim \mathcal{CN}(\mathbf{0}, \sigma_h^2\mathbf{I}_D)$:

   Since $\mathbf{h} \sim \mathcal{CN}(\mathbf{0}, \sigma_h^2\mathbf{I}_D)$,

   $$\boldsymbol{\mu} = \mathbb{E}[\mathbf{z}|\mathbf{s}] = \mathbb{E}[\mathbf{h} \otimes \mathbf{s} + \mathbf{w}|\mathbf{s}] = \mathbb{E}[\mathbf{h} \otimes \mathbf{s}|\mathbf{s}] + \mathbb{E}[\mathbf{w}|\mathbf{s}] = \mathbb{E}[\mathbf{h}] \otimes \mathbf{s} + \mathbb{E}[\mathbf{w}] = \mathbf{0} \tag{2.37}$$

   and it is shown in Appendix F that

   $$|\mathbf{C}| = (2N\sigma_h^2 + \sigma^2)^{MND} \tag{2.38}$$

   and

   $$\mathbf{C}^{-1} = \frac{1}{\sigma^2}\Big[\mathbf{I}_{MND} - \frac{1}{(\sigma^2 + 2N\sigma_h^2)}\mathbf{Q}\mathbf{Q}^H\Big] \tag{2.39}$$

where $\mathbf{Q} = \sigma_h \mathbf{I}_D \otimes \mathbf{s}$.

We can see that the determinant $|\mathbf{C}|$ is independent of $\mathbf{s}$. By maximizing and substituting in (2.33), we can see in Appendix G that the optimal decision is determined by

$$\boxed{\underset{\mathbf{s}\in\mathcal{I}_M^N}{\operatorname{argmax}} f(\mathbf{Y}|\mathbf{s}) = \underset{\mathbf{s}\in\mathcal{I}_M^N}{\operatorname{argmax}} \|\mathbf{s}^H \mathbf{Y}\|} \ . \tag{2.40}$$

Chapter 3

An Efficient Algorithm for 3-FSK and 2 Receive Antennas

In this chapter, we consider the case of 3-FSK modulation and 2 receive antennas and develop efficient algorithms for optimal noncoherent sequence detection when $\mathbf{h}$ is unknown and $\mathbf{h} \sim \mathcal{CN}(\mathbf{0}, \sigma_h^2 \mathbf{I}_D)$. By setting $M = 3$ and $D = 2$, (2.40) becomes

$$\boxed{\max_{\mathbf{s}\in\mathcal{I}_3^N} f(\mathbf{Y}|\mathbf{s}) = \max_{\mathbf{s}\in\mathcal{I}_3^N} \|\mathbf{s}^H\mathbf{Y}\| = \max_{\mathbf{s}\in\mathcal{I}_3^N} \|\mathbf{Y}^H\mathbf{s}\|}\,. \tag{3.1}$$

3.1 Theoretic Developments

3.1.1 Spherical Coordinates $\boldsymbol{\phi}$

Without loss of generality, we assume that each row of $\mathbf{Y}$ in (3.1) has at least one nonzero element, i.e., $\mathbf{Y}_{n,:} \neq \mathbf{0},\ n = 1, 2, \ldots, N$. Otherwise, the value of the variable s_n related with the all-zero row of $\mathbf{Y}$ would have no effect on the maximization procedure and could be ignored, reducing the dimension of our problem by 1.

We will now introduce the 3×1 auxiliary-angle vector $\boldsymbol{\phi} \in \Phi \triangleq (-\frac{\pi}{2}, \frac{\pi}{2}]^2 \times (-\pi, \pi]$ and

define the unit-norm 4×1 real vector

$$\tilde{\mathbf{c}}(\boldsymbol{\phi}) = \begin{bmatrix} \sin\phi_1 \\ \cos\phi_1 \sin\phi_2 \\ \cos\phi_1 \cos\phi_2 \sin\phi_3 \\ \cos\phi_1 \cos\phi_2 \cos\phi_3 \end{bmatrix} \tag{3.2}$$

and the unit-norm 2×1 complex vector

$$\mathbf{c}(\boldsymbol{\phi}) = \tilde{\mathbf{c}}_{2:2:4}(\boldsymbol{\phi}) + j\tilde{\mathbf{c}}_{1:2:3}(\boldsymbol{\phi}) = \begin{bmatrix} \cos\phi_1 \sin\phi_2 + j \sin\phi_1 \\ \cos\phi_1 \cos\phi_2 \cos\phi_3 + j \cos\phi_1 \cos\phi_2 \sin\phi_3 \end{bmatrix} . \tag{3.3}$$

From Cauchy-Schwarz Inequality, we observe that, for any $a \in \mathbb{C}^2$,

$$\Re\{\mathbf{a}^H \mathbf{c}(\boldsymbol{\phi})\} \leq \|\mathbf{a}^H \mathbf{c}(\boldsymbol{\phi})\| \leq \|\mathbf{a}\| \underbrace{\|\mathbf{c}(\boldsymbol{\phi})\|}_{=1} = \|\mathbf{a}\| . \tag{3.4}$$

Equality is achieved in both inequalities, iff $\boldsymbol{\phi}$ consists of the spherical coordinates of vector $\mathbf{a}$, i.e., iff $c(\boldsymbol{\phi}) = \frac{\mathbf{a}}{\|\mathbf{a}\|}$, since $\Re\{\mathbf{a}^H \frac{\mathbf{a}}{\|\mathbf{a}\|}\} = \|\mathbf{a}\|$. Using the above, our original problem is rewritten as

$$\boxed{\max_{\mathbf{s} \in \mathcal{I}_3^N} \|\mathbf{Y}^H \mathbf{s}\| = \max_{\mathbf{s} \in \mathcal{I}_3^N} \max_{\boldsymbol{\phi} \in \boldsymbol{\Phi}} \Re\{\mathbf{s}^H \mathbf{Y} \mathbf{c}(\boldsymbol{\phi})\} = \max_{\boldsymbol{\phi} \in \boldsymbol{\Phi}} \sum_{n=1}^{N} \max_{\mathbf{s}_n \in \mathcal{I}_3} \Re\{\mathbf{s}_n^H \mathbf{Y}_{n,:} \mathbf{c}(\boldsymbol{\phi})\}} . \tag{3.5}$$

For fixed $\boldsymbol{\phi}$, we have N single-symbol maximizations in which, for $\mathcal{M} \triangleq \{1, 2, 3\}$, every symbol is decided as

$$\boxed{\hat{\mathbf{s}}_n = \underset{\mathbf{s}_n \in \mathcal{I}_3}{\operatorname{argmax}} \Re\{\mathbf{s}_n^H \mathbf{Y}_{n,:} \mathbf{c}(\boldsymbol{\phi})\} \Leftrightarrow \hat{x}_n = \underset{x_n \in \mathcal{M}}{\operatorname{argmax}} \Re\{\mathbf{Y}_{n,:}[x_n] \mathbf{c}(\boldsymbol{\phi})\}} \tag{3.6}$$

where

$$\mathbf{Y}_{n,:}[x_n] = \mathbf{s}_n \mathbf{Y}_{n,:} \tag{3.7}$$

and

$$\mathbf{Y}_{n,:} = \begin{bmatrix} \mathbf{Y}_{n,1}[1] & \mathbf{Y}_{n,2}[1] \\ \mathbf{Y}_{n,1}[2] & \mathbf{Y}_{n,2}[2] \\ \mathbf{Y}_{n,1}[3] & \mathbf{Y}_{n,2}[3] \end{bmatrix} . \tag{3.8}$$

Finally, as it can be shown in Appendix H, the decision for x_n will change from k to l (or vice versa), with $k, l \in \mathcal{M}$ and $k \neq l$ when

$$\boxed{\mathbf{y}_n^{\{k,l\}} \tilde{\mathbf{c}}(\boldsymbol{\phi}) = 0} \tag{3.9}$$

where

$$\mathbf{y}_n^{\{k,l\}} = \begin{bmatrix} \Im\{\mathbf{Y}_{n,1}[l] - \mathbf{Y}_{n,1}[k]\} \\ \Re\{\mathbf{Y}_{n,1}[k] - \mathbf{Y}_{n,1}[l]\} \\ \Im\{\mathbf{Y}_{n,2}[l] - \mathbf{Y}_{n,2}[k]\} \\ \Re\{\mathbf{Y}_{n,2}[k] - \mathbf{Y}_{n,2}[l]\} \end{bmatrix}^T . \tag{3.10}$$

3.1.2 Surfaces $\mathcal{H}(\mathbf{y}_n^{\{k,l\}})$

According to (3.9), we can derive $\binom{M}{2}N$ different decision rules that combined separate Φ into distinct regions, each of which is uniquely associated with a different MFSK sequence. More specifically, as seen in (3.8), the decision for every symbol n depends only on the M consecutive rows of $\mathbf{Y}$ that correspond to this symbol, i.e., $\mathbf{Y}_{n,:}$. These rows determine the $\binom{M}{2}$ surfaces $\mathcal{H}(\mathbf{y}_n^{\{k,l\}})$, for $n = 1, 2, \ldots, N$ and $k, l \in \mathcal{M}$, $k \neq l$, that is 2-manifolds in 3-dimensional space, with each surface originating from two different rows of $\mathbf{Y}$. Specifically, every surfaces originates from the $\big((n-1)M + k\big)$-th and $\big((n-1)M + l\big)$-th rows of $\mathbf{Y}$ and is determined by the function

$$\phi_1 = \tan^{-1}\left(\frac{\mathbf{y}_n^{\{k,l\}}(2)\sin\phi_2 - \mathbf{y}_n^{\{k,l\}}(3)\cos\phi_2\sin\phi_3 + \mathbf{y}_n^{\{k,l\}}(4)\cos\phi_2\cos\phi_3}{\mathbf{y}_n^{\{k,l\}}(1)}\right) . \tag{3.11}$$

This can be visualized in Figure 3.1, where we can see all the surfaces originating from $\mathbf{Y}_{1,:}$, i.e., from the first $M = 3$ rows of $\mathbf{Y}$. Moreover, by solving (3.6) and visualising our data in Figure 3.2, we can see that no surface partitions our space into distinct regions continuously for every $\boldsymbol{\phi}$, but instead regions associated with each candidate symbol are created. This implies the existence of 'active' and 'inactive' parts for each surfaces and that the combination of the

'active' parts of all surfaces for a specific symbol n determines the decision boundaries for that symbol.

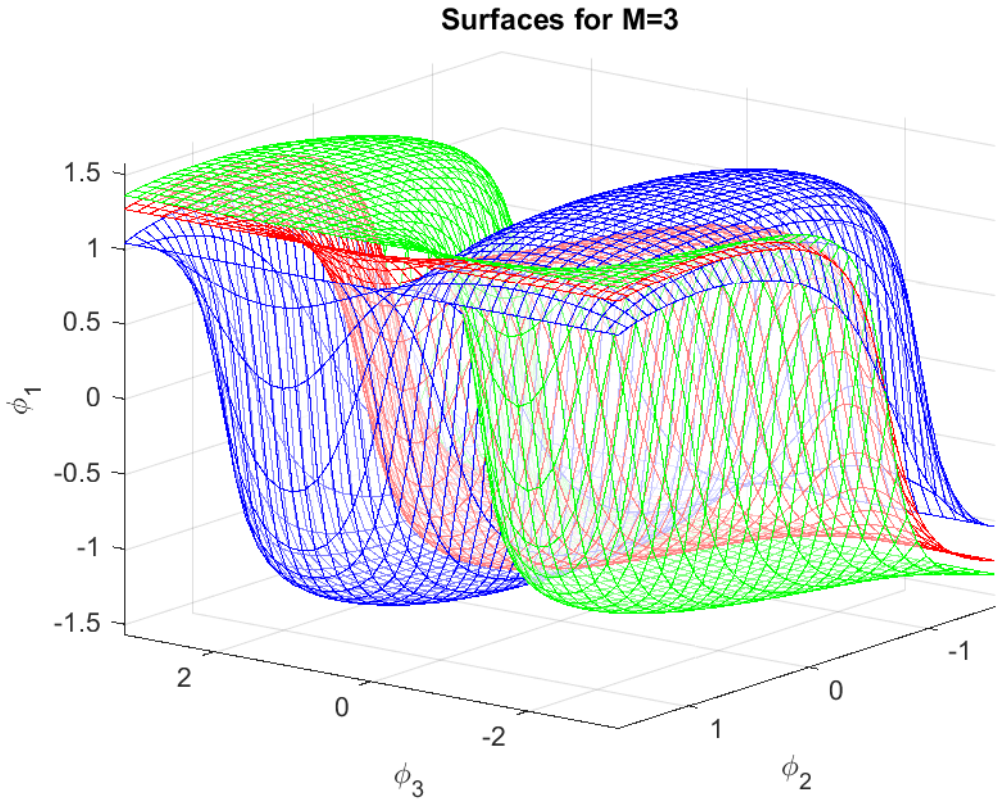

Figure 3.1: Surfaces for $M = 3$.

3.1.3 Lines & Nodes

A better and more useful visualization (of the same hypersurfaces) for the needs of this work is depicted in Figures 3.3-3.4 by setting ϕ_3 at a fixed arbitrary value, in this case $\phi_3 = -\pi$, and by plotting the now 1-manifolds in 2-dimensional space. In these figures we can see all surfaces originating from a specific symbol n, accompanied by the decision boundaries for that symbol, i.e., the 'active' parts of the surfaces originating from that symbol. This visualization will be preferred for the rest of this work and the surfaces depicted will be referred simply as **lines**.

In Figure 3.3 we can see the three lines originating from $\mathbf{Y}_{1,:}$, i.e., the line $\mathbf{y}_1^{\{1,2\}}$ that

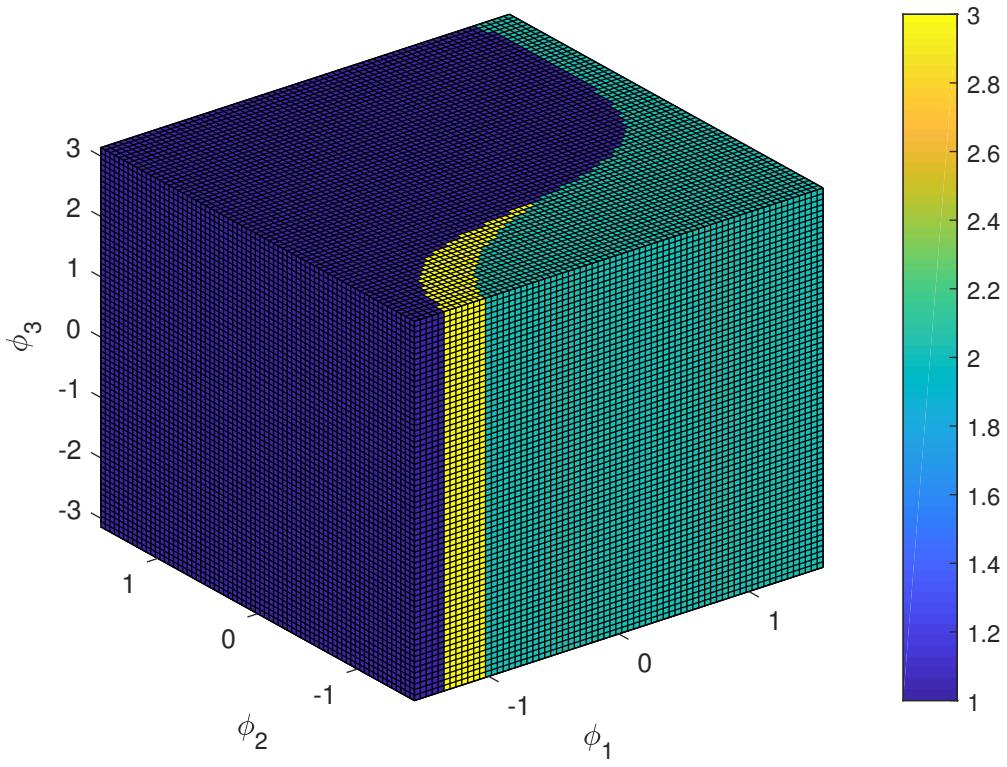

Figure 3.2: Regions created for $M = 3$.

originates from $\mathbf{Y}_{1,:}[1]$ and $\mathbf{Y}_{1,:}[2]$, the line $\mathbf{y}_1^{\{1,3\}}$ that originates from $\mathbf{Y}_{1,:}[1]$ and $\mathbf{Y}_{1,:}[3]$, and the line $\mathbf{y}_1^{\{2,3\}}$ that originates from $\mathbf{Y}_{1,:}[2]$ and $\mathbf{Y}_{1,:}[3]$. As we can see, these lines intersect at $\mathbf{A}$, with $\mathbf{A}$ constituting a vertex that 'leads' three cells, each of which is uniquely associated with a different candidate symbol. In particular, the cell between lines $\mathbf{y}_1^{\{1,2\}}$, $\mathbf{y}_1^{\{1,3\}}$ corresponds to a decision of $\hat{x}_n = 1$, the cell between $\mathbf{y}_1^{\{1,2\}}$, $\mathbf{y}_1^{\{2,3\}}$ corresponds to $\hat{x}_n = 2$, and the cell between $\mathbf{y}_1^{\{1,3\}}$, $\mathbf{y}_1^{\{2,3\}}$ corresponds to $\hat{x}_n = 3$.

These triple intersection points will be referred for the rest of this work as **nodes** and it is worth noticing that a node is formed by three lines that share in pairs of two, exactly one origination row from $\mathbf{Y}$. For example in the presented instance, lines $\mathbf{y}_1^{\{1,2\}}$, $\mathbf{y}_1^{\{1,3\}}$ have a common origin in $\mathbf{Y}_{1,:}[1]$, lines $\mathbf{y}_1^{\{1,2\}}$, $\mathbf{y}_1^{\{2,3\}}$ in $\mathbf{Y}_{1,:}[2]$ and lines $\mathbf{y}_1^{\{1,3\}}$, $\mathbf{y}_1^{\{2,3\}}$ in $\mathbf{Y}_{1,:}[3]$. So equivalently with lines that originate from two rows of $\mathbf{Y}$, every node will originate from three rows of $\mathbf{Y}$, i.e., the rows that the lines forming them originate from. In our example this means

that node $\mathbf{A}$ originates from $\mathbf{Y}_{1,:}[1]$, $\mathbf{Y}_{1,:}[2]$, and $\mathbf{Y}_{1,:}[3]$ and it can also be written as $\mathbf{A}(1,2,3)$. This is a basic property of every node and in cases with $M > 3$ will greatly affect the structure of our configuration.

We also have to mention that, even though all three lines seem to start or end at the intersection point $\mathbf{A}$, they are in fact continuous for $\phi_2 \in (-\frac{\pi}{2}, \frac{\pi}{2}]$ and we only see their 'active' and 'inactive' parts. The 'inactive' parts don't participate in the partition of Φ and are ignored.

Finally, these lines will continue to intersect for any $\hat{\phi}_3 \in (-\pi, \pi]$, with the intersection points forming a common axis in Φ. This common axis, along with the 'active' parts of $\mathbf{y}_1^{\{1,2\}}$, $\mathbf{y}_1^{\{1,3\}}$, and $\mathbf{y}_1^{\{2,3\}}$ in Φ, constitute the decision boundaries between the distinct partitioned regions of Φ.

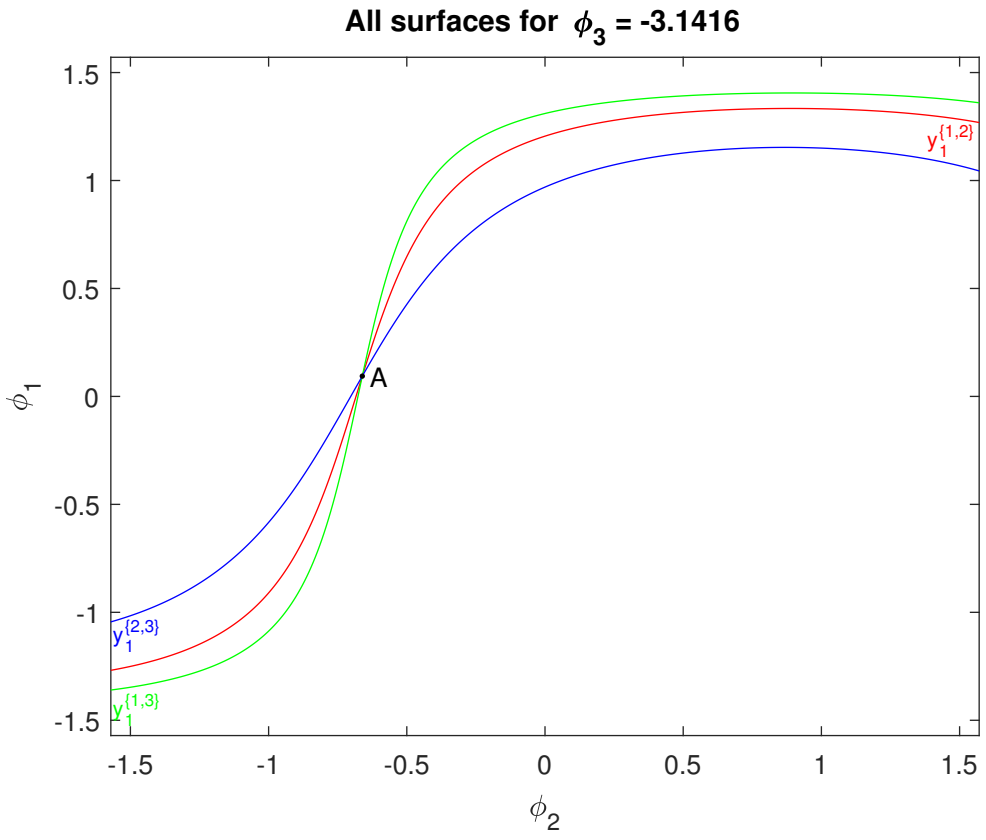

Figure 3.3: All surfaces for $\phi_3 = -\pi$.

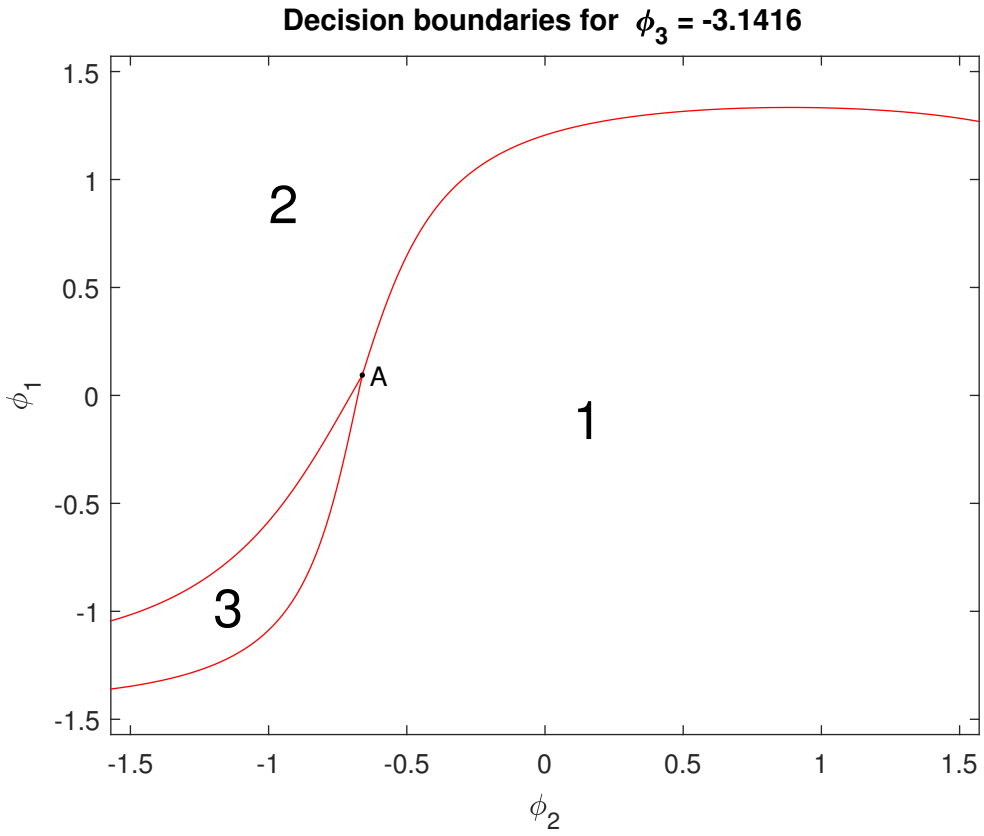

Figure 3.4: Decision Boundaries for $\phi_3 = -\pi$.

3.1.4 Sequences & Intersection Types

In the previous section we analyzed how our space is partitioned for $N = 1$ symbol and $M = 3$. We will now introduce more symbols and explore how our space is partitioned for a sequence of symbols. For N symbols and since the decision boundaries for each symbol are determined by three lines, we will now have $3N$ lines in total. All lines, if we also take into consideration their 'inactive' parts, start at $\phi_2 = -\frac{\pi}{2}$ and end at $\phi_2 = \frac{\pi}{2}$.

Moreover, as we can see in Appendix I, for fixed ϕ_3, $k, l \in \mathcal{M}$ and $\phi_2 = -\frac{\pi}{2}$, we get that

$$\boxed{\tan\phi_1 = \frac{\Re\{\mathbf{Y}_{n,1}[k] - \mathbf{Y}_{n,1}[l]\}}{\Im\{\mathbf{Y}_{n,1}[l] - \mathbf{Y}_{n,1}[k]\}}} \tag{3.12}$$

and for $\phi_2 = \frac{\pi}{2}$ that

$$\boxed{\tan\phi_1' = -\frac{\Re\{\mathbf{Y}_{n,1}[k] - \mathbf{Y}_{n,1}[l]\}}{\Im\{\mathbf{Y}_{n,1}[l] - \mathbf{Y}_{n,1}[k]\}}}\,. \tag{3.13}$$

We can see that the points that the lines cross the ϕ_1 axis for $\phi_2 = -\frac{\pi}{2}$ and $\phi_2 = \frac{\pi}{2}$ are

antisymmetric. This implies that, by contruction, all lines will eventually intersect between them for some $\hat{\phi}_3$. These intersection points can be divided into three types.

1st Type

Firsty, we have the case where three lines originating from the same symbol intersect creating nodes, as described in detail in the previous section.

2nd Type

Secondly, the case where two lines originating from different symbols intersect. Every intersection of this type will be referred for the rest of this work as **cross**, with each cross partitioning our space into four distinct candidate sequences. We can see a visualization in Figure 3.5, where the decision boundaries for $N = 2$ symbols are presented. The lines $\mathbf{y}_1^{\{1,2\}}$ and $\mathbf{y}_2^{\{1,2\}}$ are intersecting, forming the cross $\mathbf{X}_{12}^{\{1,2\},\{1,2\}}$, which partitions our space into four regions and 'leads' four cells, each associated with a different candidate sequence. Specifically, since $\mathbf{y}_1^{\{1,2\}}$ originates from $\mathbf{Y}_{1,:}[1]$ and $\mathbf{Y}_{1,:}[2]$, and $\mathbf{y}_2^{\{1,2\}}$ from $\mathbf{Y}_{2,:}[1]$ and $\mathbf{Y}_{2,:}[2]$, the four regions will correspond to the candidate sequences $\hat{\mathbf{s}} = 11$, $\hat{\mathbf{s}} = 12$, $\hat{\mathbf{s}} = 21$ and $\hat{\mathbf{s}} = 22$.

Equivalently with the lines, crosses will also be 'active' or 'inactive', depending on whether they are formed by the 'active' or the 'inactive' parts of the lines constituting them. We can easily deduct that in order for a cross to change its status it will have to 'meet' a node for some ϕ_3 and that the only nodes available for a cross to 'meet' are those with whom they share one line. 'Active' crosses and nodes 'lead' cells and now partition Φ into distinct regions, each of which is uniquely associated with a different MFSK sequence.

Returning to Figure 3.5, the only nodes that the cross $\mathbf{X}_{12}^{\{1,2\},\{1,2\}}$ can 'meet' are $\mathbf{A}_1(1,2,3)$ and $\mathbf{B}_2(1,2,3)$. We can see this happening in Figure 3.6, where cross $\mathbf{X}_{12}^{\{1,2\},\{1,2\}}$ 'meets' with node $\mathbf{A}_1(1,2,3)$, i.e., all lines that are participating in forming $\mathbf{X}_{12}^{\{1,2\},\{1,2\}}$ and $\mathbf{A}_1(1,2,3)$ are intersecting between them for some $\phi_3 \in [-\pi, \pi)$. This also equivalent to $\mathbf{A}_1(1,2,3)$ 'meeting'

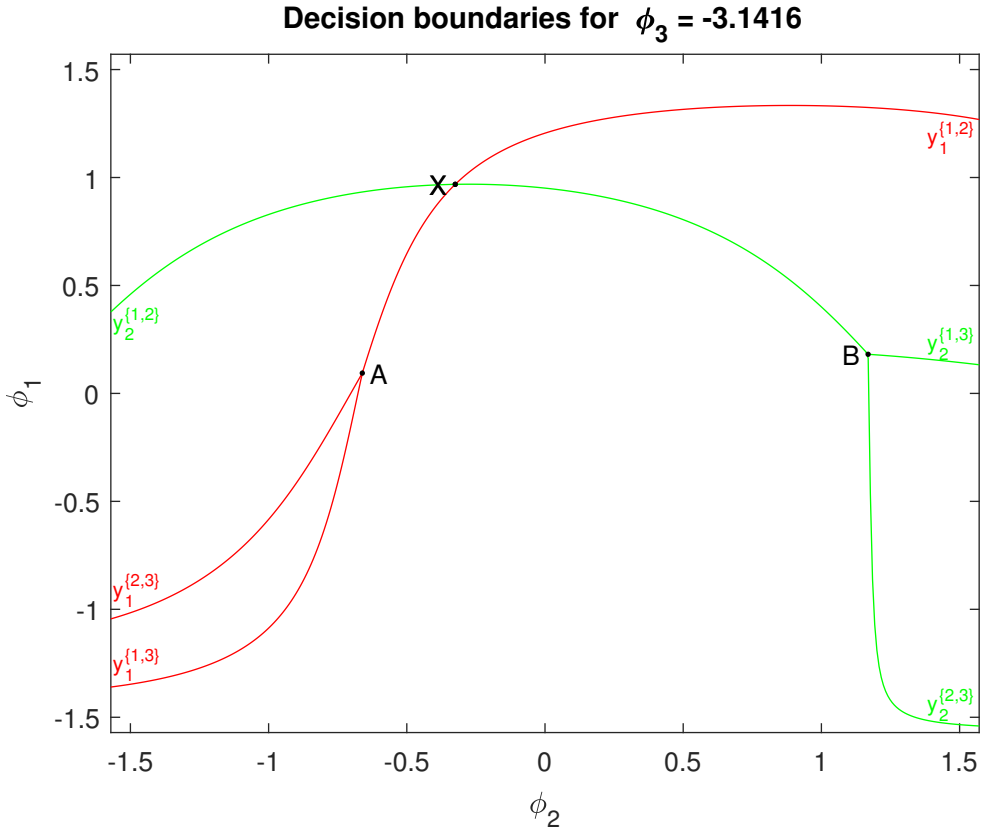

Figure 3.5: Decision boundaries for $\phi_3 = -\pi$.

$\mathbf{y}_2^{\{1,2\}}$, through $\mathbf{y}_1^{\{1,2\}}$.

In Figure 3.7, the same case is presented for some $\hat{\phi}_3 > \phi_3$, where a new cell has now been created, i.e., a new possible candidate 'appears'. The cross $\mathbf{X}_{12}^{\{1,2\},\{1,2\}}$ has turned 'inactive' and no longer 'leads' any cell, but it's worth noticing here that even though $\mathbf{X}_{12}^{\{1,2\},\{1,2\}}$ no longer 'leads' any cells, these cells are still 'active' and that new crosses are 'appearing', i.e., are turning 'active'. These two new crosses, along with the node that participated in the intersection, will now 'lead' the previous cells, as well as the newly created cell. The new 'active ' crosses are formed by the remaining lines of the participating node, i.e., $\mathbf{y}_1^{\{1,3\}}$ and $\mathbf{y}_1^{\{2,3\}}$, intersecting with the line originating from the second symbol, i.e., $\mathbf{y}_2^{\{1,2\}}$.

In our example, crosses $\mathbf{Y}_{12}^{\{2,3\},\{1,2\}}$ and $\mathbf{Z}_{12}^{\{1,3\},\{1,2\}}$ turn 'active' and now each 'lead' four cells out which they share exactly two, while one of these cells is actually the newly created cell. In order to identify these two cells and their associated candidates sequences, we firstly have

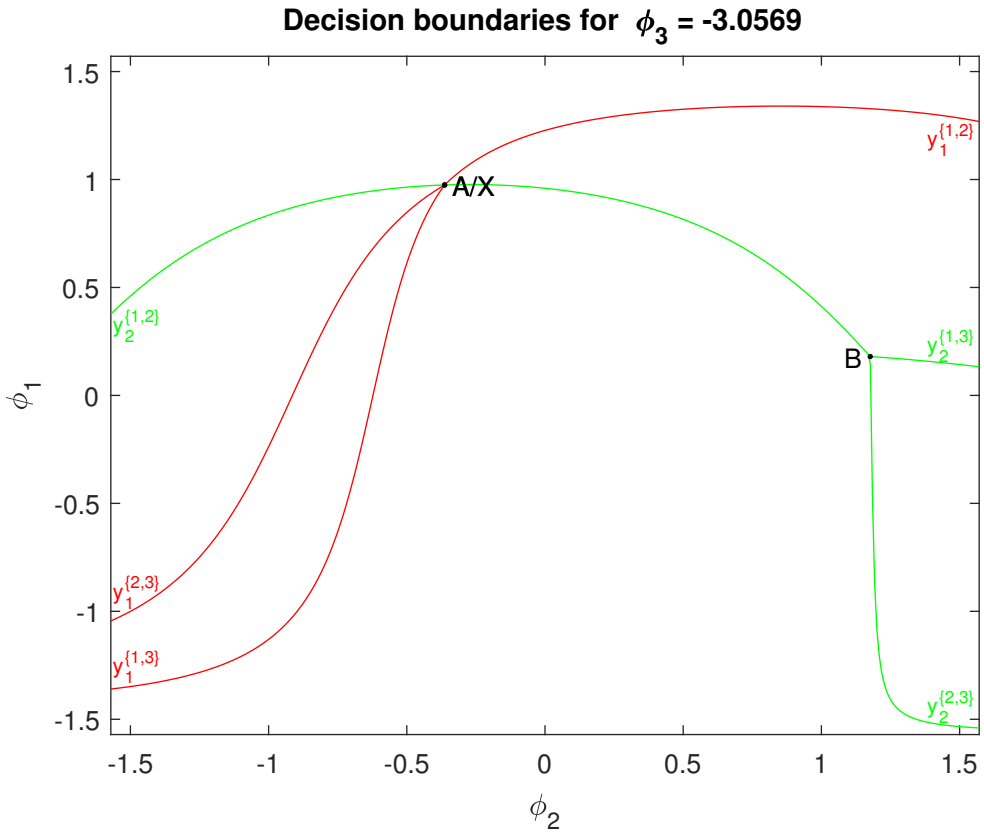

Figure 3.6: Decision boundaries for $\phi_3 = -3.0569$.

to identify the lines forming the participating node for the first symbol and then we have to search for the ones that form 'active' crosses with the line originating from the second symbol. The common origination row these lines share will correspond to the correct candidate symbol. If a cell had closed instead, in order to identify this cell we just need to find the lines of the participating node that now form 'inactive' crosses with the line originating from the second symbol. The common origination row these lines share will again correspond to the correct candidate symbol. In our case a new cell is created, while $\mathbf{y}_1^{\{1,3\}}$ and $\mathbf{y}_1^{\{2,3\}}$ are the lines that now form 'active' crosses with $\mathbf{y}_2^{\{1,2\}}$ and since they both originate from $\mathbf{Y}_{1,:}[3]$, the correct candidate symbol is $\hat{x}_1 = 3$. Hence, the two associated candidates are $\hat{\mathbf{s}} = 31$ and $\hat{\mathbf{s}} = 32$.

While we can easily identify the correct one visually, distinguishing between the two candidates will be a source of ambiguity in our algorithm. We can resolve this ambiguity, either by evaluating the metric of the second symbol at the spherical coordinates determined by the

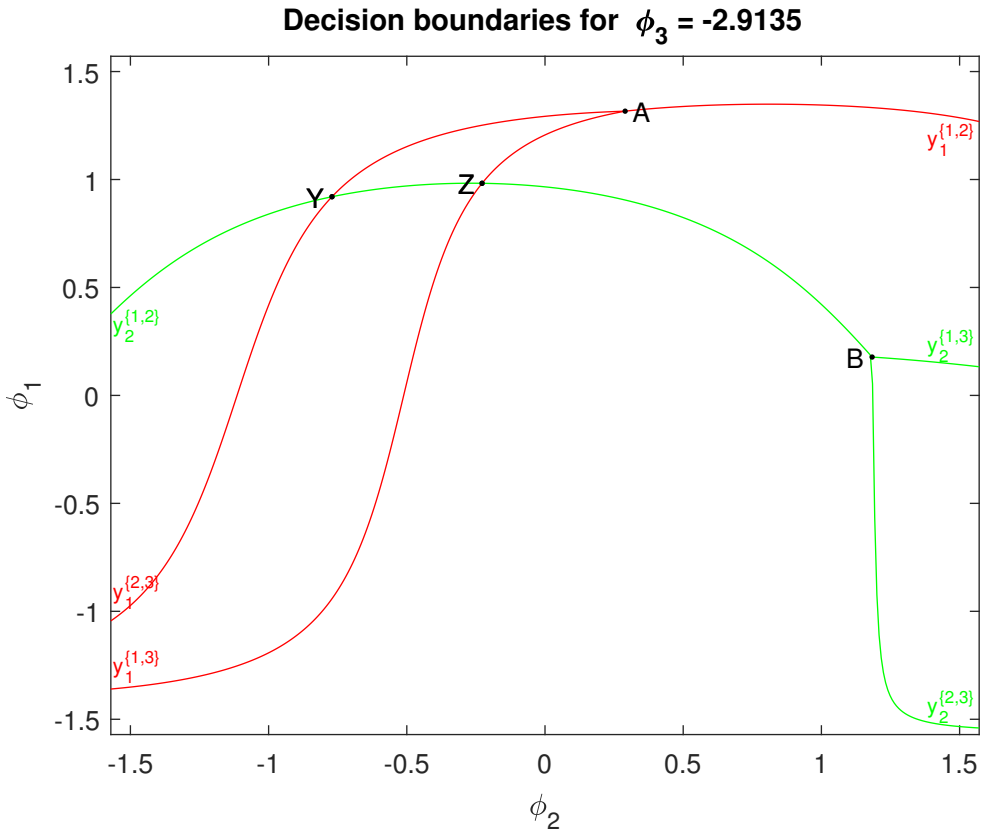

Figure 3.7: Decision boundaries for $\phi_3 = -2.9135$.

intersection of all lines originating for the first symbol, i.e., the spherical coordinates of node $\mathbf{A}_1(1,2,3)$ in our example, or simply by evaluating both candidates against our metric, trading off this way reductancy for simplicity. In our case, the newly created cell is actually associated with the candidate sequence $\hat{\mathbf{s}} = 32$.

If $\mathbf{Y}_{12}^{\{2,3\},\{1,2\}}$ and $\mathbf{Z}_{12}^{\{1,3\},\{1,2\}}$ were initially 'active' instead, due to the structure of our configuration they would 'meet' with $\mathbf{A}_1(1,2,3)$ at the same ϕ_3 and they would both turn 'inactive', while $\mathbf{X}_{12}^{\{1,2\},\{1,2\}}$ would turn 'active'. This would also be equivalent to the 'inactive' cross $\mathbf{X}_{12}^{\{1,2\},\{1,2\}}$ 'meeting' with $\mathbf{A}_1(1,2,3)$ for that ϕ_3, as in fact all lines originating from the first symbol will intersect with $\mathbf{y}_2^{\{1,2\}}$ for that ϕ_3. In this scenario the cell associated with the candidate sequence $\hat{\mathbf{s}} = 32$ would close.

When $N > 2$, in order for us to identify the remaining candidate symbols of the sequence that is 'appearing' (or 'disappearing') due to the meeting of a node with a cross, we just need to

find the spherical coordinates of the intersection point and by using (3.6) calculate the winning candidate for every other symbol, besides the two participating in this intersection. We can also generalize that every time a cross 'meets' with a node, if the cross is initially 'active' it changes to 'inactive' and a new cell is created. Otherwise, if the cross was initially 'inactive' it changes to 'active' and the cell closes.

3rd Type

Finally, we have to mention another type of intersections that may occur while we traverse ϕ_3, that is when three lines originating from different symbols intersect, i.e., three crosses 'meet'. By contruction, every cross can only 'meet' a neighbouring cross, i.e., a cross with whom they share exactly one line and no other cross or node can be found between them. When these intersections occur, one cell associated with a candidate sequences closes, while another one (its complementary) opens. We can identify these cells and associated candidate sequences by firstly identifying the aforementioned intersections points and the lines that participate in them.

In Figures 3.8-3.10 we can see an example of this type of intersections, where the crosses $\mathbf{X}_{12}^{\{1,3\},\{1,3\}}$, $\mathbf{Y}_{13}^{\{1,3\},\{2,3\}}$ and $\mathbf{Z}_{23}^{\{1,3\},\{2,3\}}$ intersect for some ϕ_3. The lines that participate are $\mathbf{y}_1^{\{1,3\}}$, $\mathbf{y}_2^{\{1,3\}}$ and $\mathbf{y}_3^{\{2,3\}}$. As we can see, after the intersection one cell is replaced by a new one and since these cells are complementary, it suffices for us to identify only one cell. In order to do that, we first need to notice that these cells take the form of 'triangles', with the every cross playing the part of a corner. We can also notice that, by construction, one of the cells will always be 'under' the decision boundaries originating from two of our symbols and 'over' the decision boundary originating from the remaining symbol, while the other one will always be 'over' the decision boundaries originating from two of our symbols and 'under' the decision boundary originating from the remaining symbol. We can identify this remaining symbol, by setting $\phi_2 = -\pi/2$ or

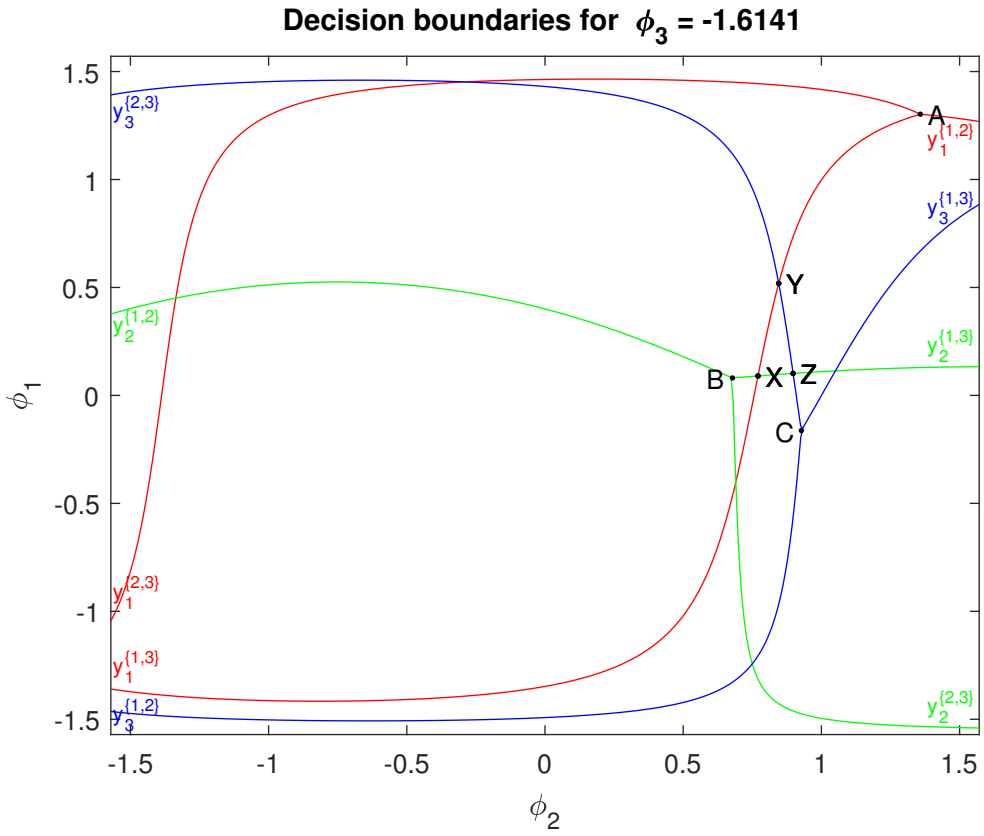

Figure 3.8: Decision boundaries for $\phi_3 = -1.6141$.

$\phi_2 = \pi/2$, i.e., find the points that every line crosses the ϕ_1-axis. Then the line that we are searching for is the one that is inbetween the other two lines, i.e., the second in sorted by ϕ_1 order, as this line will always be either 'above', or 'under' the cross formed by the other two lines for any $\phi_3 \in [-\pi, \pi)$. We will call this line the **base line** of our 'triangle'. If one line is 'inactive' for $\phi_2 = -\pi/2$, then we consider instead the point that the 'inactive' part crosses the ϕ_1-axis, which is antisymmetric to the point that the 'active' part crosses the ϕ_1-axis for $\phi_2 = \pi/2$. Equivalently, if one line is 'inactive' for $\phi_2 = \pi/2$, then we consider instead the antisymmetric point that the 'inactive' part crosses the ϕ_1-axis for $\phi_2 = -\pi/2$.

We can now identify both candidates, as every candidate sequence will be either 'over' the base line and 'under' the remaining two lines, or 'under' the base line and 'over' the remaining two. In our example, as we mentioned the participating lines are $\mathbf{y}_1^{\{1,3\}}$, $\mathbf{y}_2^{\{1,3\}}$ and $\mathbf{y}_3^{\{2,3\}}$. We can set $\phi_2 = \pi/2$ and check the order in which the lines cross the ϕ_1-axis, considering also

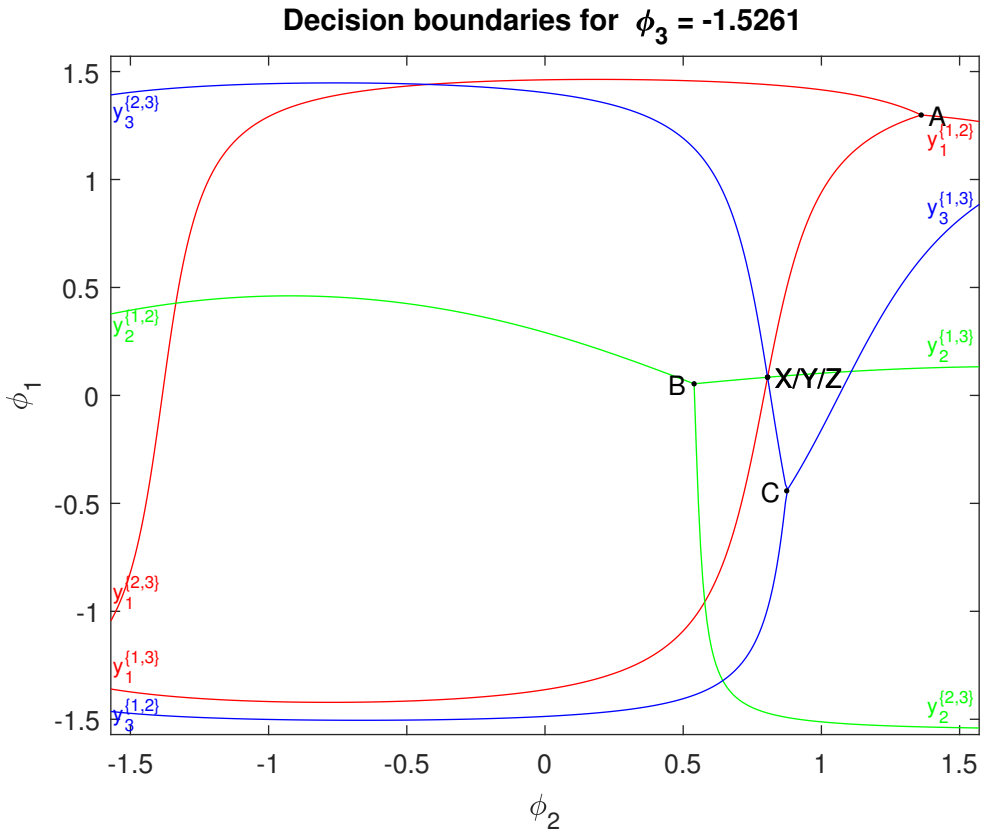

Figure 3.9: Decision boundaries for $\phi_3 = -1.5261$.

the 'inactive' part of $\mathbf{y}_3^{\{2,3\}}$. The base line is the line originating from the second symbol, i.e., $\mathbf{y}_2^{\{1,3\}}$, which means that the candidates that correspond to the two complementary cells in our partition will be either $\hat{\mathbf{s}} = 313$ 'over' the base line, or $\hat{\mathbf{s}} = 132$ 'under' the base line.

Finally, we can combine the set of all candidates created by the intersection types described in this chapter, with the set of candidate sequences that their associated cells 'touch' the ϕ_1-axis, therefore never 'disappear'. This way we can have the complete set of candidate sequences whose associated cells 'appear' in $\mathbf{\Phi}$.

3.2 Algorithmic Developments

As we explained in the previous section, in order to get the complete set of candidate sequences, it suffices to identify the spherical coordinates of the points where new cells 'appear' (or 'disappear'), find the associated candidate sequences and combine them with the set of

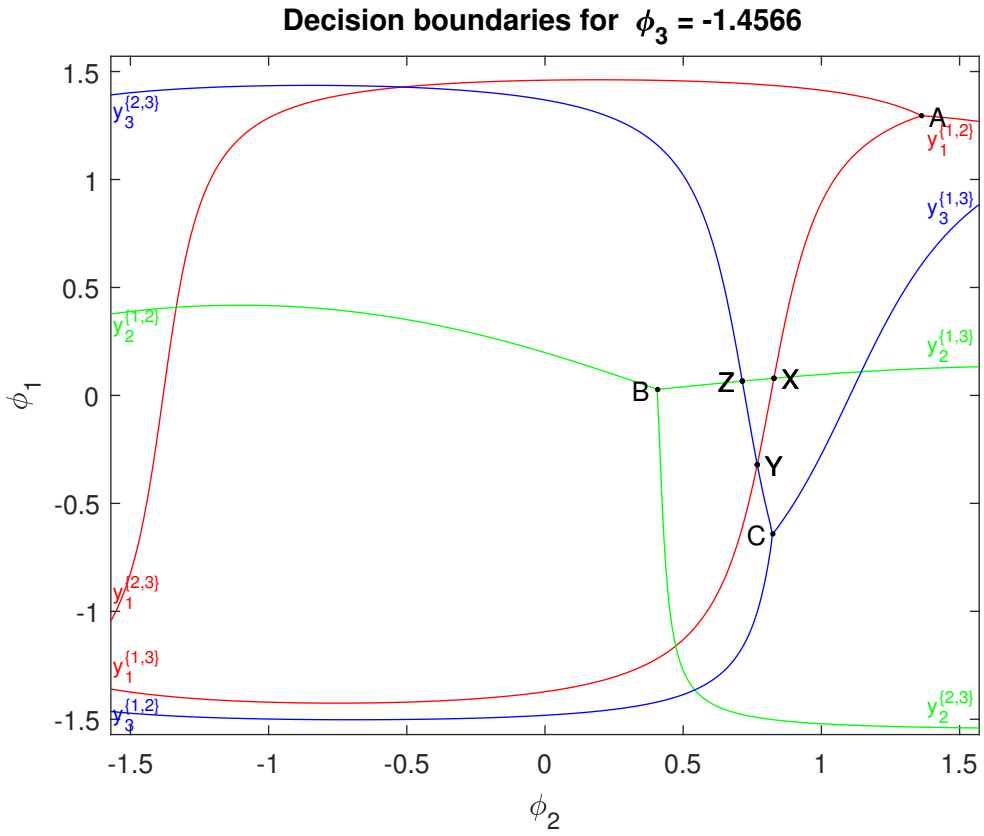

Figure 3.10: Decision boundaries for $\phi_3 = -1.4566$.

candidates associated with the cells that are always open. New cells can 'appear' (or 'disappear') either when a node 'meets' with cross, which is also equivalent to a node 'meeting' with a line originating from a different symbol, or when three lines originating from different symbols intersect, which is also equivalent to three neighbouring 'active' crosses meeting.

The first case is more predictable as by construction every node will eventually 'meet', for some ϕ_3, every other line that originates from another symbol. This means that for any input, we can always identify $3N(N-1)$ 'meeting' points where a cell will 'appear' (or 'disappear'). As every cell (besides the ones touching the $\phi 1_1$-axis) will eventually close, we are interested only in the closing cases when identifying a candidate sequence. Also when a node 'meets' a line, it is the only way for the participating crosses to change their activity status. We will identify, sort by ϕ_3, and save the spherical coordidates of these points to a $3 \times (3N^2 - 3N)$ matrix, in order to visit them serially.

In the second case the number of intersections cannot be predicted, but for an intersection to be valid the participating crosses will have to be 'active'. Firstly we have to identify and store all the 'active' crosses for $\phi_3 = -\pi$ in a $3N \times 3N$ matrix , where every row and column are associated with a different line. Since all these crosses won't change their status as long as a node doesn't 'meet' a line, only these crosses can participate in the creation of new cells. Moreover, a cross can only 'meet' another cross with whom it shares a line, i.e., they are stored in the same row or column of the aforementioned matrix. Also, a cross can only 'meet' a 'neighbouring' cross, i.e., no other cross can be found between them. We can easily find the order of the crosses by sorting them by phi_2. We can then try all cross combinations that satisfy the aforementioned criteria, check if their 'meeting' point is valid, i.e., the 'active' parts of the participating lines intersect for that $\boldsymbol{\phi}$ and in that case save the spherical coordinates $\boldsymbol{\phi}$ of that triple intersection point. This way we can find all initial possible 'triangles.'

These triple intersections may also happen before the next node-line 'meeting'point and since we are using the node-line 'meeting' points as our fixed 'checkpoints'', we may skip this way cells that are associated with 'triangles' that 'appear' and 'disappear' before the next node-line 'meeting' point. For this reason, we will also need to visit these intersections points first and identify again all possible 'triangles' for each participating cross, as described in the previous paragraph.

Then, when a node finally 'meets' a line and our 'active' nodes change, we update our matrix and repeat the previous process using only the new 'active' crosses, which as explained in the previous section will be either one (if a cell 'disappears') or two (if a cell 'appears'). We may identify our candidate sequences only if a cell is 'disappearing', but we need to keep in mind that the activity status of the crosses is still changing.

In both previous cases, every time a new candidate sequence is produced we calculate its metric, compare it with the maximum metric we have found until then and save it if the

new metric is greater than the maximum. That way we avoid storing all possible candidates, thus saving memory. After we have traversed all ϕ_3, all that is left is to evaluate also our trivial candidates, i.e., the ones associated with the cells that never close. As mentioned before, these are the cells that 'touch' the ϕ_1-axis and we can easily identify the associated candidate sequences, by arbitrarily choosing a point on the ϕ_1 axis between every two consecutive lines (originating from different symbols). This produces $3N$ possible candidates, which we then evaluate against our maximum metric.

Algorithm 1 The Proposed Algorithm for $M = 3$

Find the spherical coordinates of all the points that a node 'meets' with a line, sort them by ϕ_3 in ascending order and store them in the $3 \times 3N(N-1)$ matrix *srt_hits*.
Find all 'active' crosses for $\phi_3 = -\pi$ and store them in the $3N \times 3N$ matrix *ngb*.
Find all initial 'triangles', sort them by ϕ_3 in ascending order and store them in *triangles*.
$i \leftarrow 1$;
$end\_flag \leftarrow false$;
while $i \leq 1 : 3N(N-1)$ **do**
    if (there is no valid 'triangle' before $srt\_hits(i)$) & ($end\_flag = false$) **then**
        $cur \leftarrow srt\_hits(i)$;
        if *cur* corresponds to a cell closing **then**
            Identify associated candidate sequences and evaluate them against our metric.
        end if
        Update *ngb* with the new 'active' and 'inactive' crosses.
        for every new 'active' cross **do**
            Find all new valid 'triangles', store them to *triangles* and sort *triangles* by ϕ_3 in ascending order.
        end for
        if $i = 3N(N-1)$ **then**
            $end\_flag \leftarrow true$;
        else
            $i++$;
        end if
    else
        if !isEmpty(*triangles*) **then**
            $cur \leftarrow triangles(1)$;
            Identify associated candidate sequences and evaluate them against our metric.
            Remove current 'triangle' from *triangles*.
            Find all new valid 'triangles', store them to *triangles* and sort *triangles* by ϕ_3 in ascending order.
        else if (isEmpty(*triangles*)) & ($end\_flag = true$) **then**
            $i++$;
        end if
    end if
end while
Find all trivial candidates and evaluate them against our max metric.
Return the candidate sequence associated with the final winner metric.

3.3 Complexity Analysis

Spatial Complexity

As explained in the previous section, it is necessary to keep track of all the spherical coordinates that a node will 'meet' a line. This would require a $3 \times (3N^2 - 3N)$ matrix for a spatial complexity of $\mathcal{O}(N^2)$. We also need to keep track of the 'active' crosses by using a $3N \times 3N$ matrix, again for a spatial complexity of $\mathcal{O}(N^2)$. These are the most memory-requiring parts of the algorithm, as we avoid saving all possible candidate sequences. All other vectors and matrices that our implementation uses, will require a spatial complexity of at most $\mathcal{O}(N)$. Our total spatial complexity will then be in the order of $\mathcal{O}(N^2)$.

Time Complexity

Finding the spherical coordinates of a point will require constant time. This means that in order to find all 'meeting' points, $3N(N-1)$ iterations will be necessary, for a time complexity of $\mathcal{O}(N^2)$. We will then need to sort these points, with the time required been $\mathcal{O}(\log 3N(N-1)) = \mathcal{O}(\log N)$. Finding all 'active' crosses will require finding $\binom{3N}{2}$ combinations of lines and evaluating their validity. Validity check will require constant time, so the time the whole procedure requires will be $\mathcal{O}(N^2)$. Next step is to visit all $3N(N-1)$ 'meeting' points. In every iteration we need to identify and evaluate the associated candidate sequence, which can be done in constant time. Updating *crs* matrix also can be done in constant time, as at most four of its cells will be affected in every iteration. The crosses correspoding to these cells are the only ones that we need to check for their 'meeting' points and as explained in the previous section they can only 'meet' with crosses on the same row or column of *crs*. As every row and column can have $3N$ elements, we will need to visit at most $4 \cdot 3N$ cells in every iteration, for a total time complexity of $\mathcal{O}(12N3N(N-1)) = \mathcal{O}(N^3)$. We finally need

to identify our trivial candidates, which as we mentioned already will be $3N$. Visiting all of them then will require $\mathcal{O}(N)$. Our implementation does present some 'hidden' costs due to the operations required, but none of them will be greater than $\mathcal{O}(N^3)$. Therefore our algorithm is dominated by that cost and our overall time complexity will be $\mathcal{O}(N^3)$.

Chapter 4

Insights Towards An Efficient M-FSK Algorithm for 2 Receive Antennas

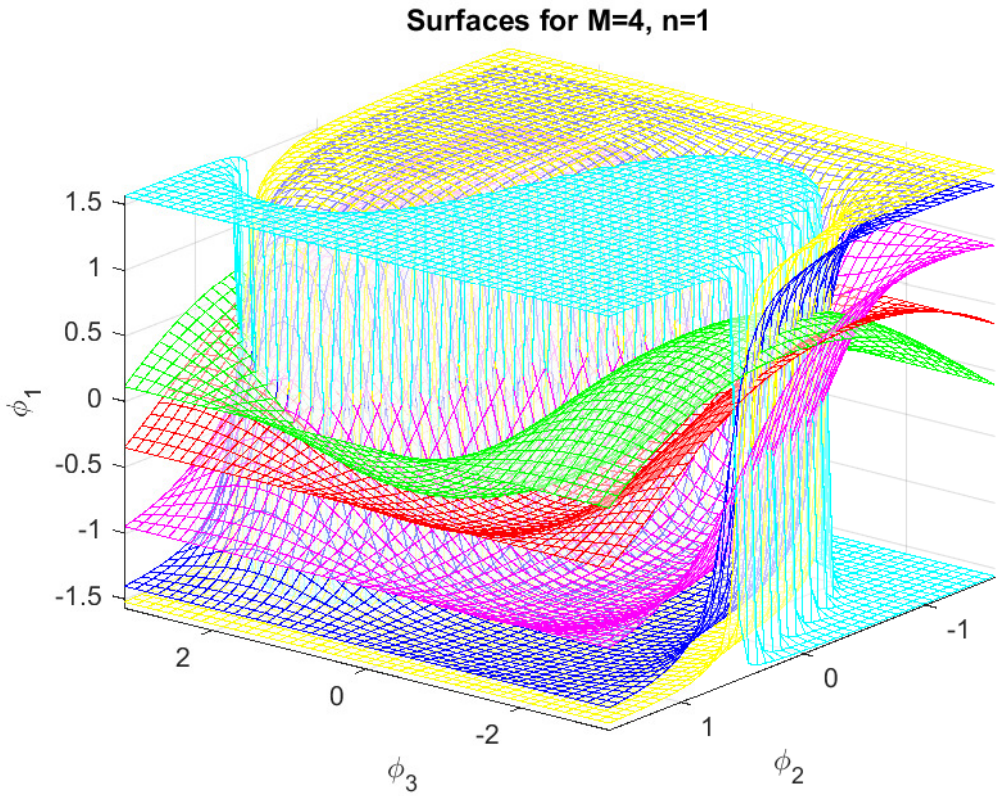

Figure 4.1: Surfaces for $M = 4, n = 1$.

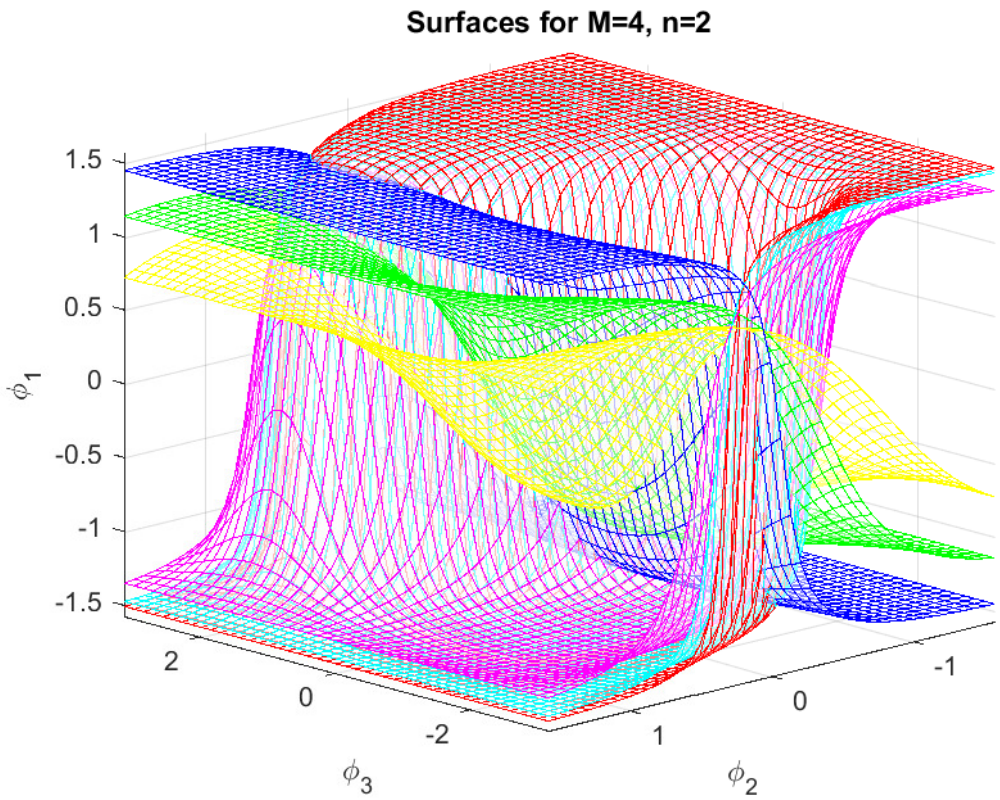

Figure 4.2: Surfaces for $M = 4, n = 2$.

4.1 The $M = 4$ Case

We will examine the $M = 4$ case building on what was observed for $M = 3$. As explained, one node will partition our space into three distinct regions associated with a candidate symbol. We can expect that in order to add one extra partition to our space, we will need to add another node to our configuration. This can only happen if the two nodes share exactly one line. Moreover, as every node is the intersection of three lines, joining the two nodes through a shared line will force the remaining lines to intersect between them, thus creating new nodes that may, or may not 'lead' a cell associated with a candidate symbol, depending on whether the intersecting lines are 'active'. Also, if every line originates from two rows of $\mathbf{Y}$ and every node originates from three rows of $\mathbf{Y}$, then since the two joining nodes share one line, they must share exactly two origination rows of $\mathbf{Y}$ and in each node this leaves room for only one more possible origination row, for a total of four different rows of $\mathbf{Y}$, i.e., four distinct candidate

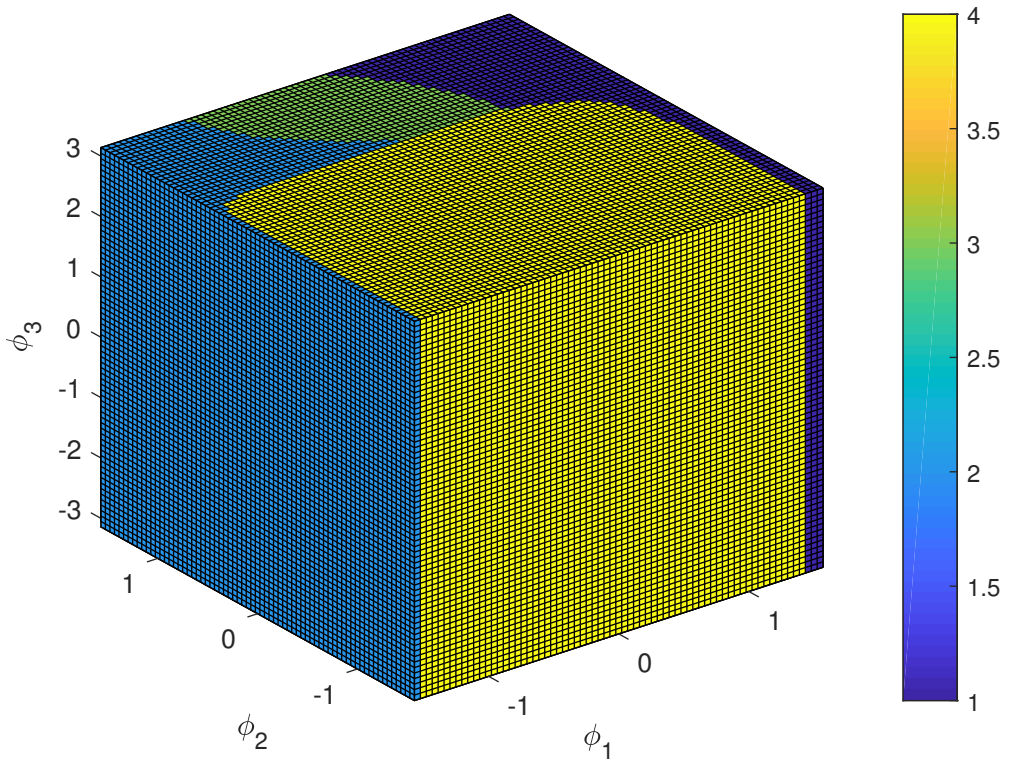

Figure 4.3: Regions created for $M = 4, n = 1$.

symbols. Finally, it's worth noticing that a $M = 4$ partition can also be intepreted as two distinct $M = 3$ cases, joined together. We also present in Figures 4.1-4.4 a $M = 4$ case, for two different symbols, where we can see all surfaces for every symbol n and the regions created when solving (3.6).

We can confirm the aforementioned claims firstly by inspecting Figure 4.6, where we can see the node $\mathbf{B}(1,3,4)$ partitioning our space into three distinct regions associated with candidates $\hat{x}_n = 1$, $\hat{x}_n = 3$ and $\hat{x}_n = 4$ and the node $\mathbf{C}(2,3,4)$ partitioning our space into three distinct regions associated with candidates $\hat{x}_n = 2$, $\hat{x}_n = 3$ and $\hat{x}_n = 4$. In this case $\mathbf{B}(1,3,4)$ is joining $\mathbf{C}(2,3,4)$ through $\mathbf{y}_1^{\{3,4\}}$, with both nodes still 'leading' three regions each. In Figure 4.5 we can also see the 'inactive' nodes $\mathbf{D}(1,2,3)$ and $\mathbf{E}(1,2,4)$, that we can also imagine as being created by joining $\mathbf{B}(1,3,4)$ and $\mathbf{C}(2,3,4)$, thus forcing $\mathbf{y}_1^{\{1,2\}}$, $\mathbf{y}_1^{\{1,3\}}$, $\mathbf{y}_1^{\{2,3\}}$ and $\mathbf{y}_1^{\{1,2\}}$, $\mathbf{y}_1^{\{1,4\}}$, $\mathbf{y}_1^{\{2,4\}}$ to intersect.

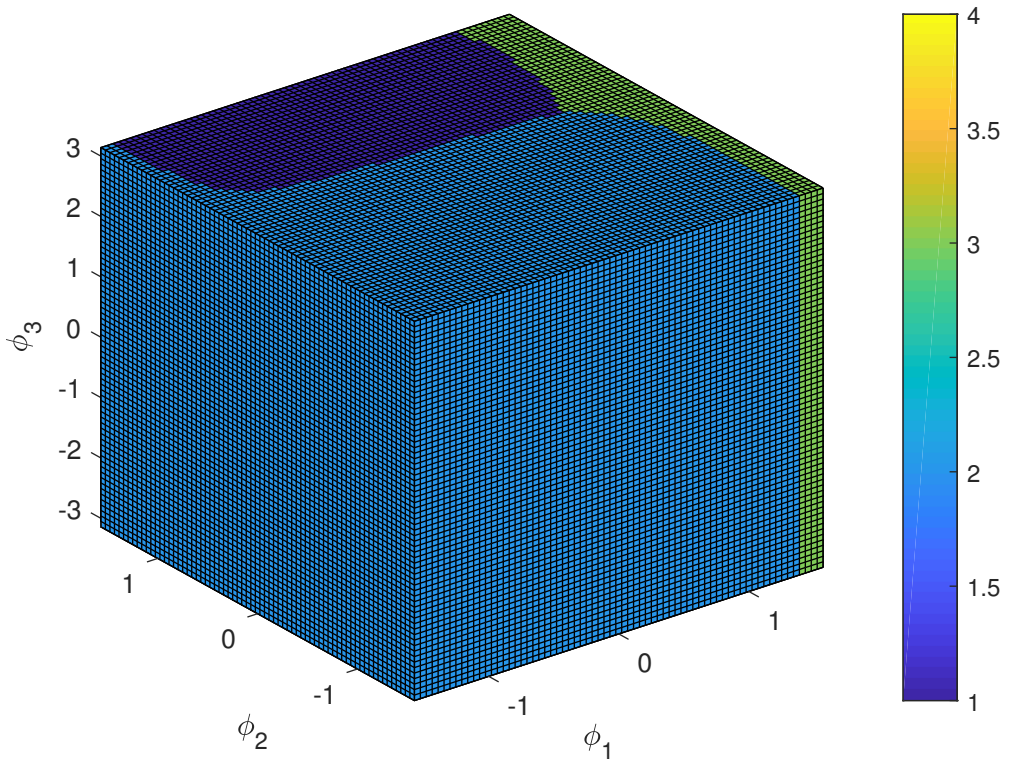

Figure 4.4: Regions created for $M = 4, n = 2$.

In Figures 4.7-4.8 we can see another case for $M = 4$, where only $\mathbf{F}$(1,2,3) 'leads' a cell and partitions our space into three distinct regions associated with candidates $\hat{x}_n = 1$, $\hat{x}_n = 2$ and $\hat{x}_n = 3$, while nodes $\mathbf{G}$(1,2,4), $\mathbf{H}$(1,3,4) and $\mathbf{I}$(2,3,4) remain 'inactive'. This is worth mentioning, as it becomes apparent that it is not necessary for our space to be partitioned in exactly $M = 4$ distinct regions for every $\boldsymbol{\phi} \in \boldsymbol{\Phi}$.

Finally, we can see that a configuration of 6 lines and 4 nodes in total is required, which agrees with the number of lines and nodes that we would theoretically expect to need, as we would have available $M = 4$ rows of $\mathbf{Y}$ to either create lines by using them in pairs, i.e $\binom{4}{2} = 6$ lines, or to create nodes by using them in triplets, i.e., $\binom{4}{3} = 4$ nodes.

We also present in Figures 4.9-4.12 the same surfaces and decision boundaries for $\phi_3' = \phi_3 + \pi$, where it's worth noticing that the surfaces are antisymmetric, but the same doesn't apply for the decision boundaries. This implies again that for $M > 3$ the 'active' parts will

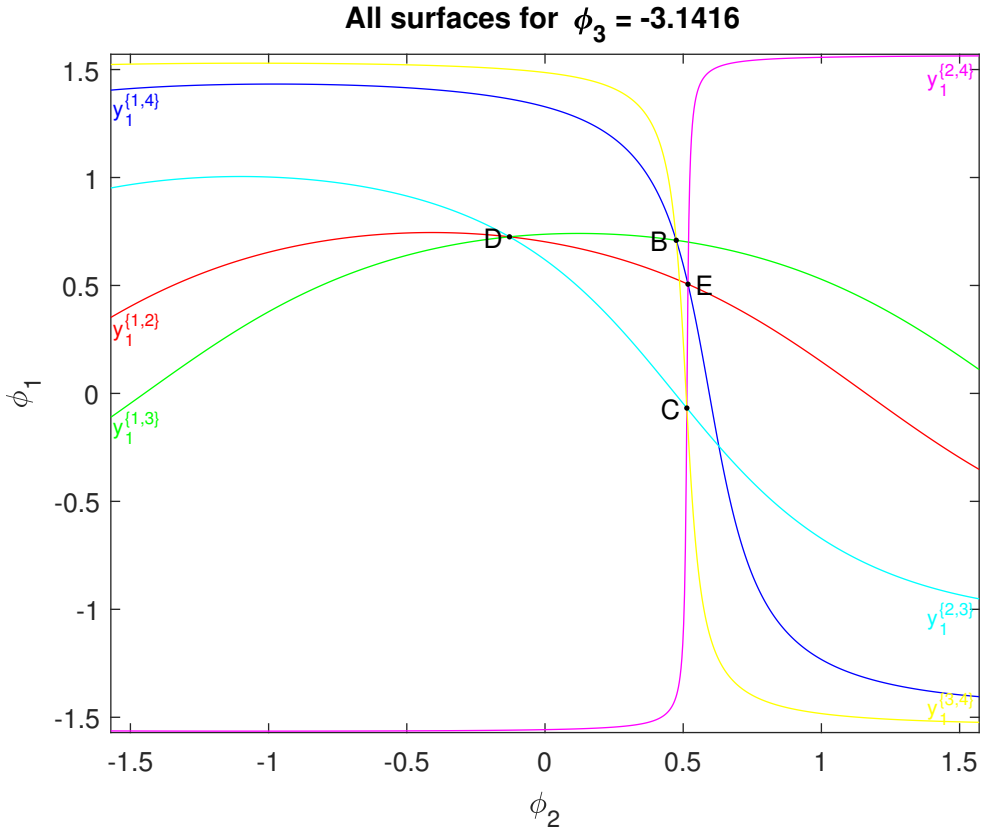

Figure 4.5: All surfaces for $\phi_3 = -\pi$.

change for some $\boldsymbol{\phi}$, changing this way also the decision boundaries.

By traversing ϕ_3, all lines will eventually intersect (or equivalently all nodes will 'meet' between them) for some $\hat{\phi}_3$ and at that point 'active' and 'inactive' nodes will change their statuses. In Figures 4.9-4.10 the nodes **B**(1,3,4) and **C**(2,3,4) are now 'inactive', when nodes **D**(1,2,3) and **E**(1,2,4) are the current 'active' nodes that 'lead' cells and partition our space in our distinct regions. This means that there is a $\hat{\phi}_3$ that all nodes 'meet', or that all six lines intersect. Also, equivalently with before, we can imagine this partition as nodes **D**(1,2,3) and **E**(1,2,4) joining together through $\mathbf{y}_1^{\{1,2\}}$, thus creating also the 'inactive' nodes **B**(1,3,4) and **C**(2,3,4). In Figures 4.11-4.12 we can see that our space is now partioned in four regions and that the three nodes **G**(1,2,4), **H**(1,3,4) and **I**(2,3,4) are now 'active', while node **F**(1,2,3) is 'inactive'. Again, all lines intersected for some $\hat{\phi}_3$ and at that point the status of the nodes changed. We can also imagine this configuration as nodes **H**(1,3,4) and **I**(2,3,4) joining together

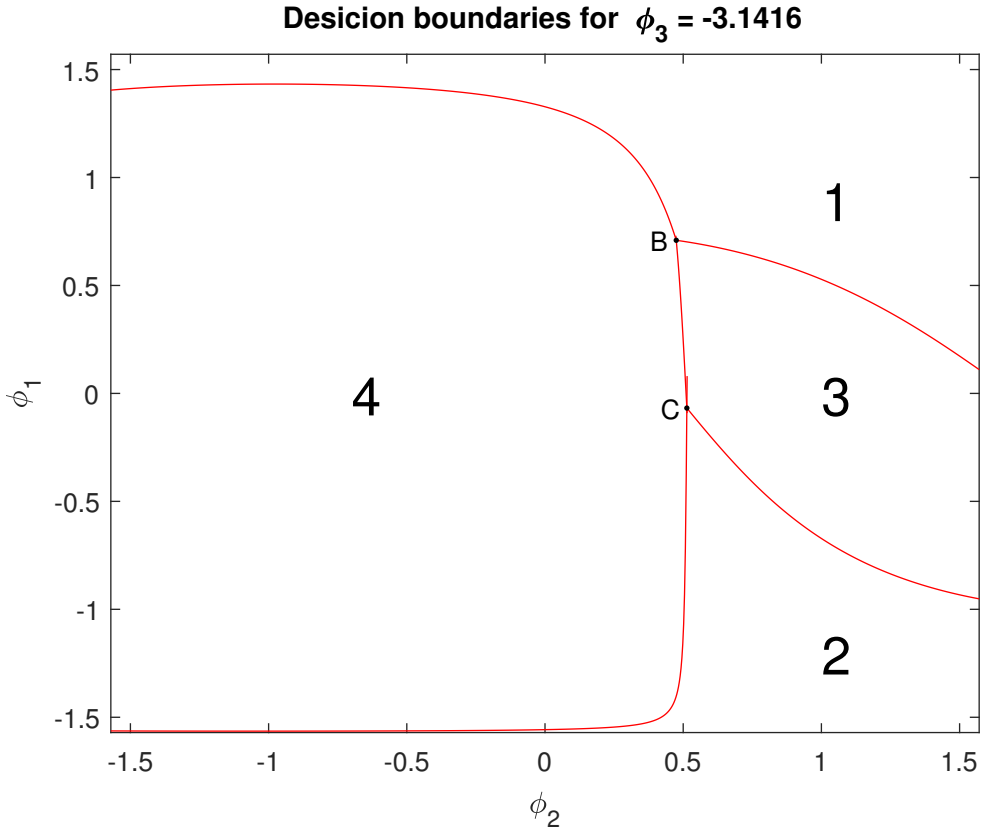

Figure 4.6: Decision boundaries for $\phi_3 = -\pi$.

through $\mathbf{y}_2^{\{3,4\}}$, thus creating the 'active' node $\mathbf{G}(1,2,4)$ and the 'inactive' node $\mathbf{F}(1,2,3)$.

The configurations that were presented in this section cover all possible configurations that may appear when partitioning our space for $M = 4$, due to the way that each individual node is built, as when two nodes join through a shared lined, the ways that the remaining lines are forced to intersect is fixed by construction.

4.2 The $M \in \mathbb{N}_{\geq 2}$ Case

Based on the $M = 4$ case, we can generalize our observations for any $M \in \mathbb{N}_{\geq 2}$. In any case our decision boundaries will always be derived from the 'active' lines and nodes. As we explained, every time our space needs to be partitioned in one extra region, one more node needs to be joined through a shared line. For example, by building on the $M = 4$ case we can create a partition of five regions by joining one more node. When joining these two nodes

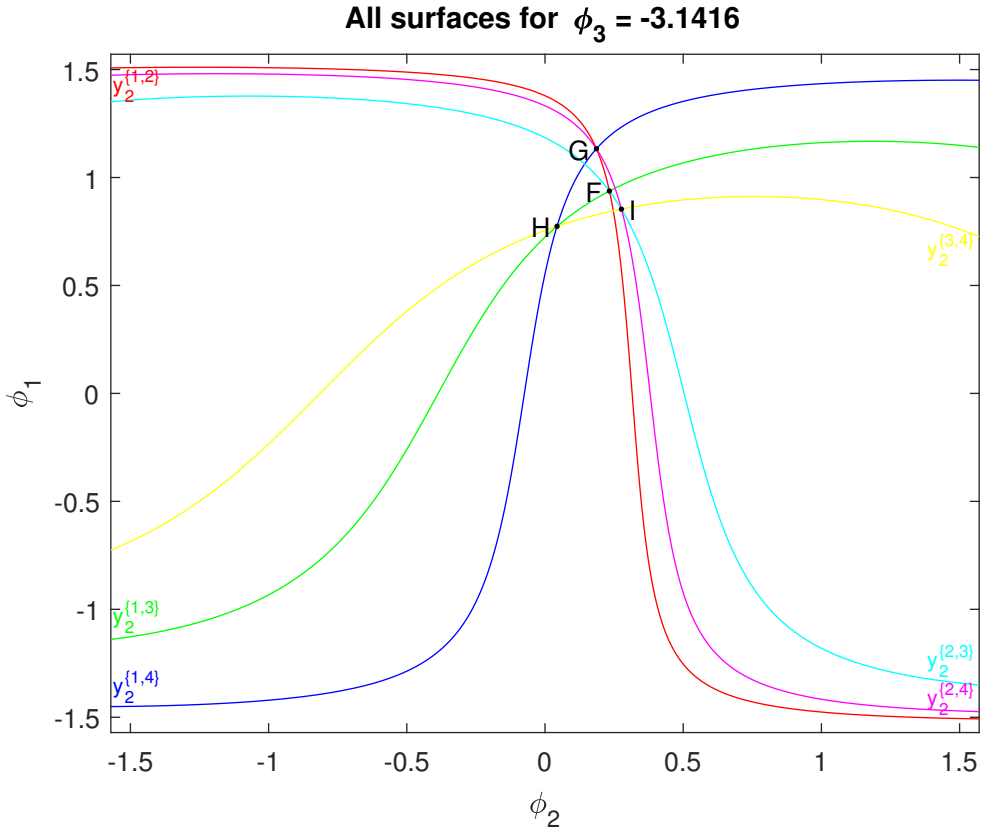

Figure 4.7: All surfaces for $\phi_3 = -\pi$.

we can ignore the remaining nodes and treat our case as explained before for $M = 4$. This way we can take advantage of the fixed number of possible configurations that may appear for $M = \{3, 4\}$ and use this property to build configurations for any $M \in \mathbb{N}_{\geq 2}$, i.e., treat every $M > 4$ case as many $M = \{3, 4\}$ cases joint together.

Equivalently with the $M = 4$ case, the nodes that 'lead' a cell will only change when the six lines forming the cell, intersect for some $\hat{\phi}_3$ or equivalently when the four nodes that 'lead' the cell 'meet', iff at least one of the nodes involved is 'active' at that time. In total there can be $2\binom{M}{4}$ such intersections (as each one will happen twice), with only half of them leading to a change of the nodes that 'lead' a cell. We can generalize also that for any M it is not necessary for our space to be partitioned in exactly M distinct regions for every $\boldsymbol{\phi} \in \boldsymbol{\Phi}$. The total number of lines needed can always be found by $\binom{M}{2}$ and the total number of nodes involved by $\binom{M}{3}$.

A visual representation of a partition of space for $M = 5$ is presented in Figures 4.13-4.16,

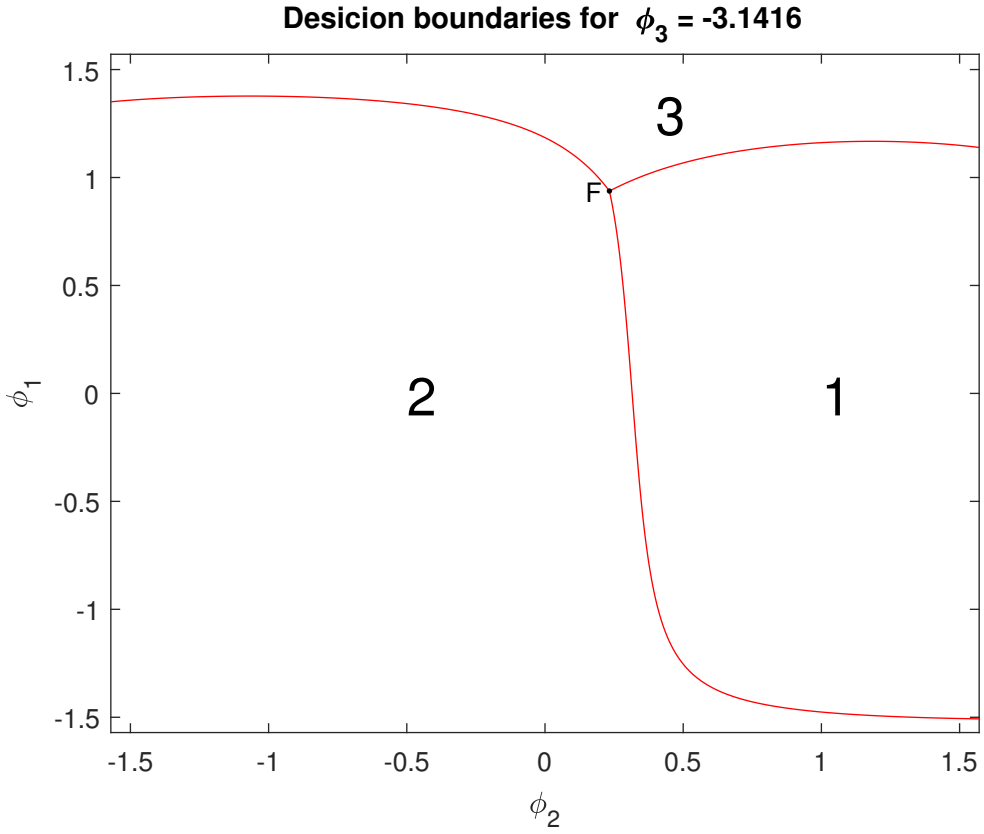

Figure 4.8: Decision boundaries for $\phi_3 = -\pi$.

where we can also confirm the validity of the aforementioned claims. In Figures 4.13-4.14 we can see the two active nodes $\mathbf{M}(1,3,4)$ and $\mathbf{J}(1,2,3)$, out of a total of $\binom{5}{3} = 10$ nodes created by $\binom{5}{2} = 10$ lines that partition our space into four distinct regions. This is also equivalent to joining two $M = 3$ cases through $\mathbf{y}^{\{1,3\}}$. InFigures 4.15-4.16 we present the same example for $\phi_3' = \phi_3 + \pi$ and we can see that the 'active' nodes have now changed to $\mathbf{L}(1,2,5)$, $\mathbf{R}(2,4,5)$, $\mathbf{O}(1,4,5)$ and $\mathbf{P}(2,3,4)$ and partition our space into five distinct regions. This is now also equivalent to joining one $M = 3$ case with one $M = 4$ case, i.e., joining $\mathbf{P}(2,3,4)$ and $\mathbf{R}(2,4,5)$ through $\mathbf{y}^{\{2,4\}}$.

4.3 Algorithmic Insights

The algorithm presented in the previous chapter ca be generalized for any $M \in \mathbb{N}_{\geq 2}$ as the only thing that changes for $M > 3$ is the addition of more nodes per symbol. In an equivalent

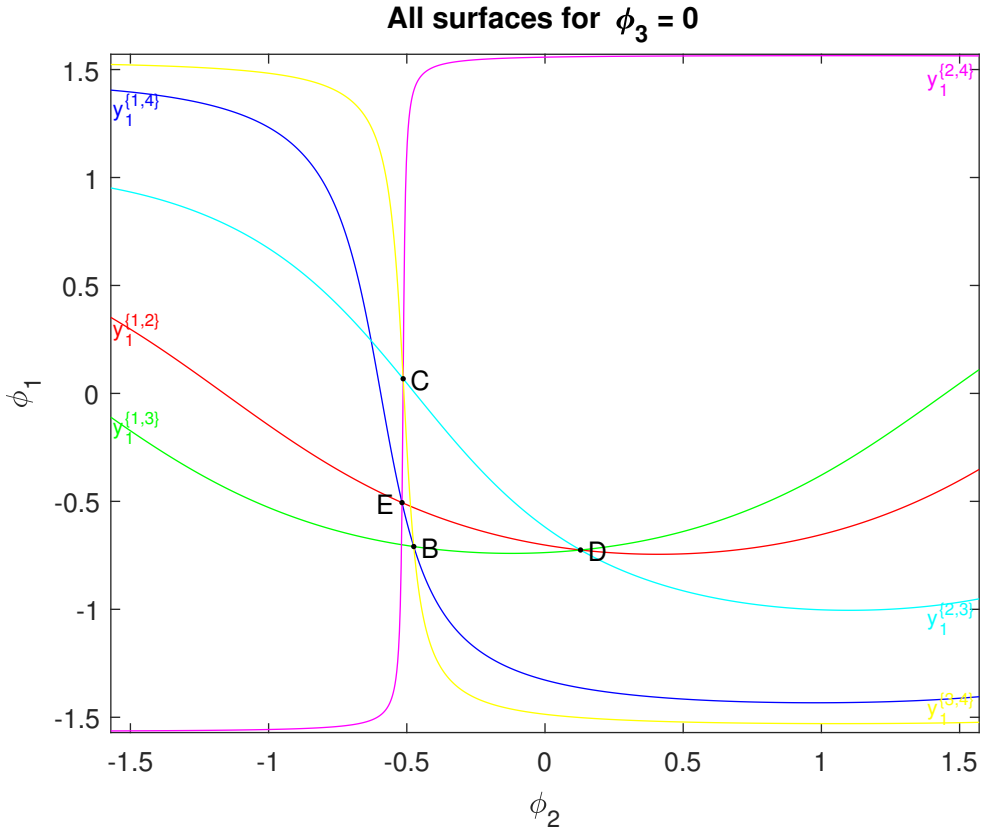

Figure 4.9: All surfaces for $\phi_3 = 0$.

way with the $M = 3$ case, we will have again to search for the spherical coordinates of the 'meeting' points between nodes and lines originating from different symbols, or for the valid intersections of three lines originating from different symbols. What needs to be considered though, is that for $M > 3$ we can have 'active' and 'inactive' nodes. This means that the aforementioned 'meeting' points will also have to be evaluated for their validity, i.e., only an 'active' node 'meeting' a line will produce a new candidate. This would require from us to also keep track of the spherical coordinates of the points that the status of a node changes, i.e., when six lines originating from the same symbol intersect, as explained in the previous chapter.

4.4 Further Development Opportunities for $D > 2$

As explained, our proposed algorithm is only developed for $D = 2$, since otherwise it would be impossible to visualize our developments. Nevertheless, it can be fully generalized

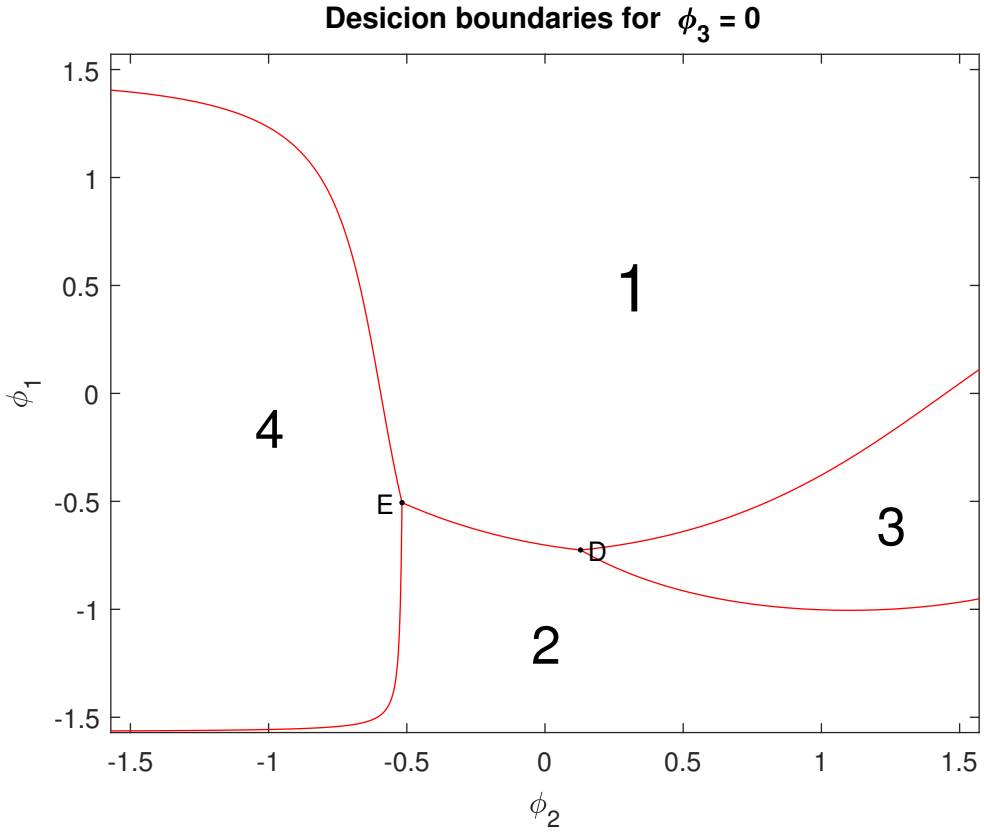

Figure 4.10: Decision boundaries for $\phi_3 = 0$.

for any $D > 2$ by replacing the auxiliary-angle and unit-norm vectors introduced in (**3.1.1**). Any possible future developments would have to start by introducing instead the $(2D-1) \times 1$ auxiliary-angle vector $\boldsymbol{\phi} \in (-\frac{\pi}{2}, \frac{\pi}{2}]^{2D-2} \times (-\pi, \pi] \triangleq \Phi$ and then by defining the unit-norm $2D \times 1$ real vector

$$\tilde{\mathbf{c}}(\boldsymbol{\phi}) = \begin{bmatrix} \sin\phi_1 \\ \cos\phi_1 \sin\phi_2 \\ \cos\phi_1 \cos\phi_2 \sin\phi_3 \\ \vdots \\ [\prod_{i=1}^{2D-2} \cos\phi_i] \sin\phi_{2D-1} \\ [\prod_{i=1}^{2D-2} \cos\phi_i] \cos\phi_{2D-1} \end{bmatrix} \tag{4.1}$$

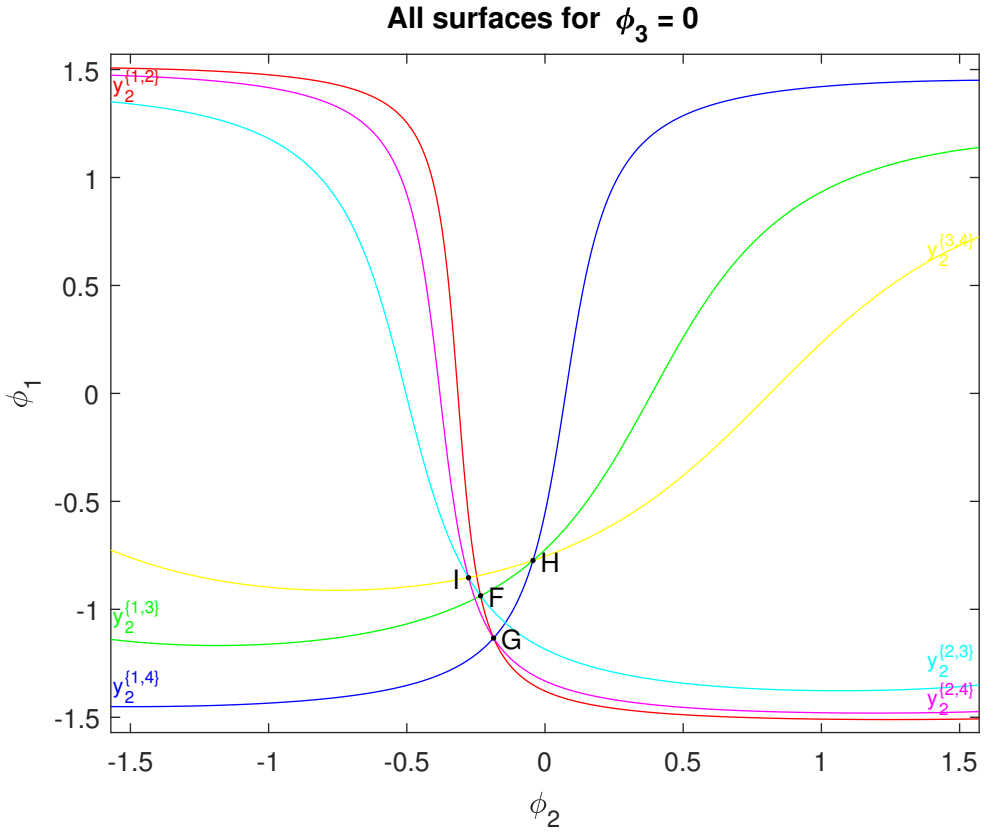

Figure 4.11: All surfaces for $\phi_3 = 0$.

and the unit-norm $D \times 1$ complex vector

$$\mathbf{c}(\boldsymbol{\phi}) = \tilde{\mathbf{c}}_{2:2:2D}(\boldsymbol{\phi}) + j\tilde{\mathbf{c}}_{1:2:2D-1}(\boldsymbol{\phi}) = \begin{bmatrix} \cos\phi_1 \sin\phi_2 + j \sin\phi_1 \\ \cos\phi_1 \cos\phi_2 \cos\phi_3 \sin\phi_4 + j \cos\phi_1 \cos\phi_2 \sin\phi_3 \\ \vdots \\ [\prod_{i=1}^{2D-2} \cos\phi_i] \cos\phi_{2D-1} + j[\prod_{i=1}^{2D-2} \cos\phi_i] \sin\phi_{2D-1} \end{bmatrix}. \tag{4.2}$$

In this generalized case, the surfaces introduced in (**3.1.2**) would be replaced by hypersurfaces instead, that is $(2D-2)$-manifolds in $(2D-1)$-dimensional space, with each hypersurface originating from two different rows of $\mathbf{Y}_{n,:}$.

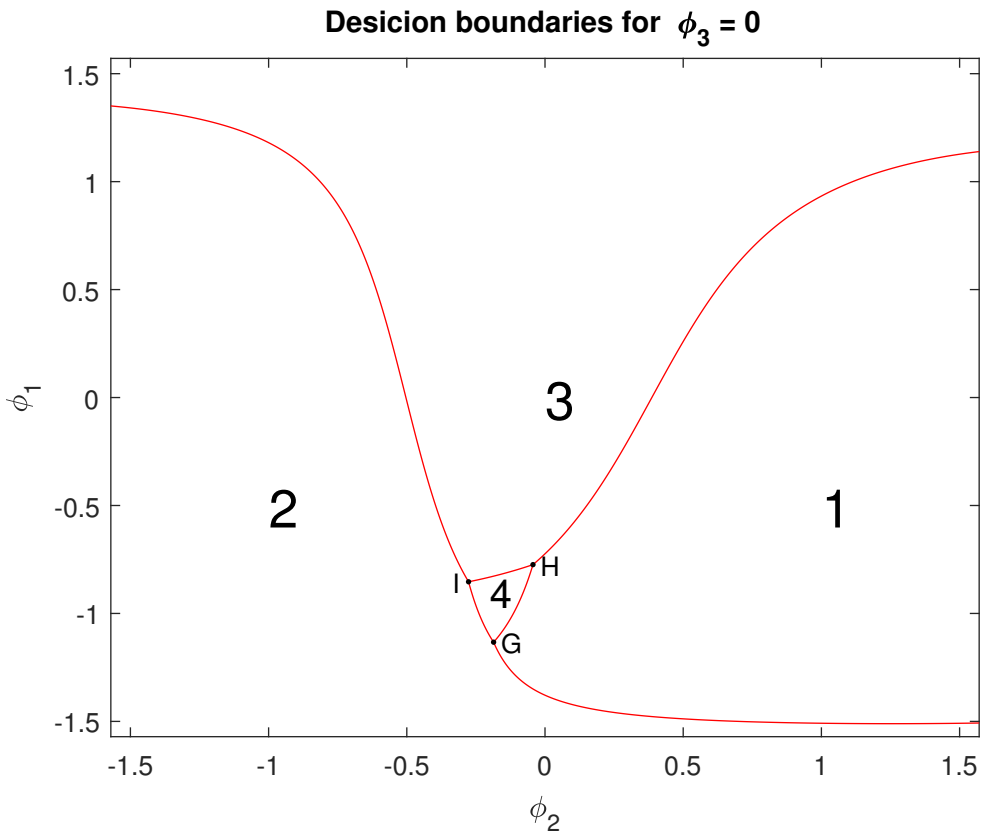

Figure 4.12: Decision boundaries for $\phi_3 = 0$.

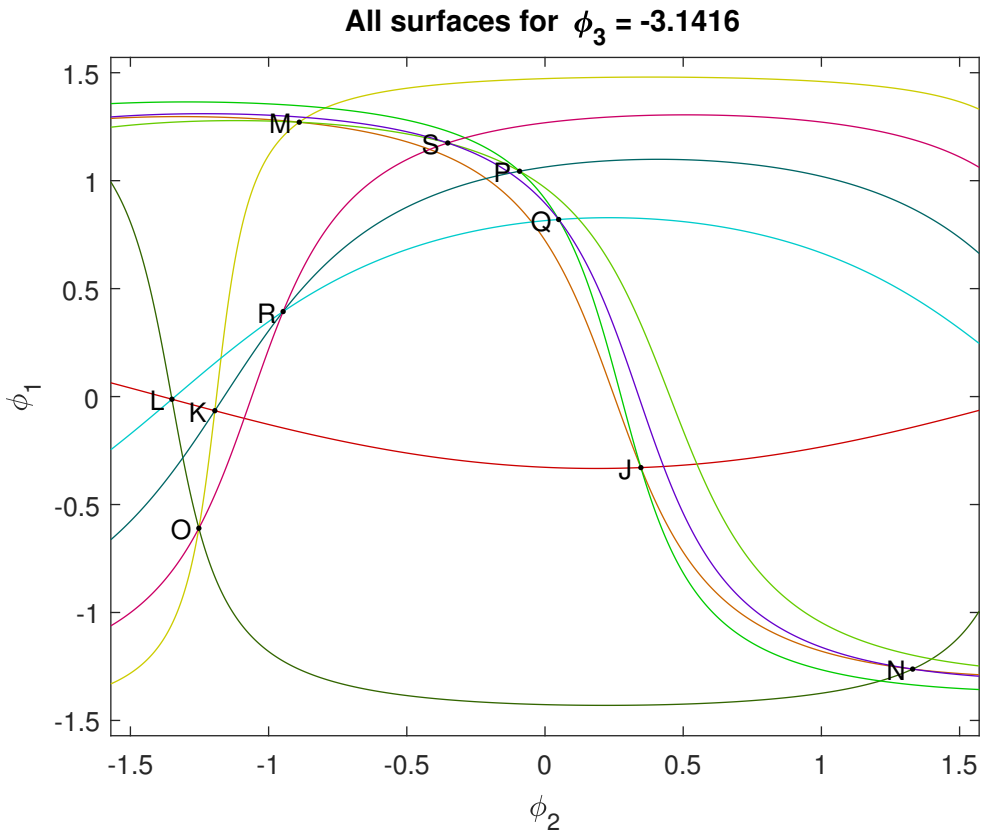

Figure 4.13: All surfaces for $\phi_3 = -\pi$.

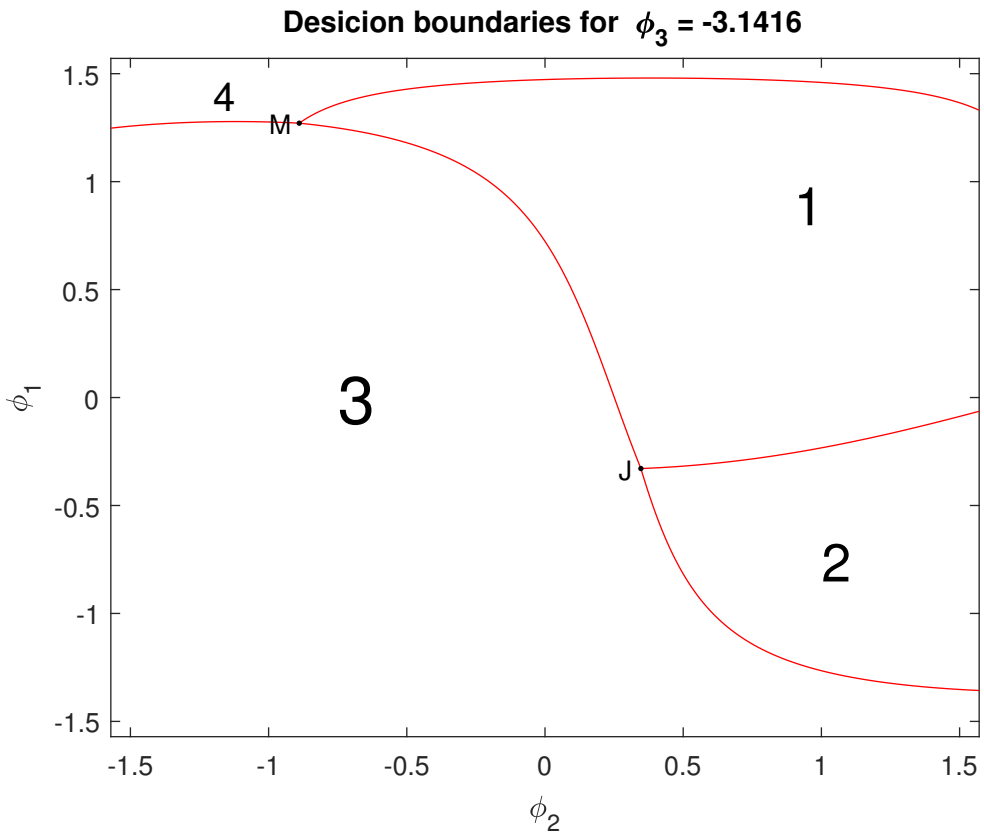

Figure 4.14: Decision boundaries for $\phi_3 = -\pi$.

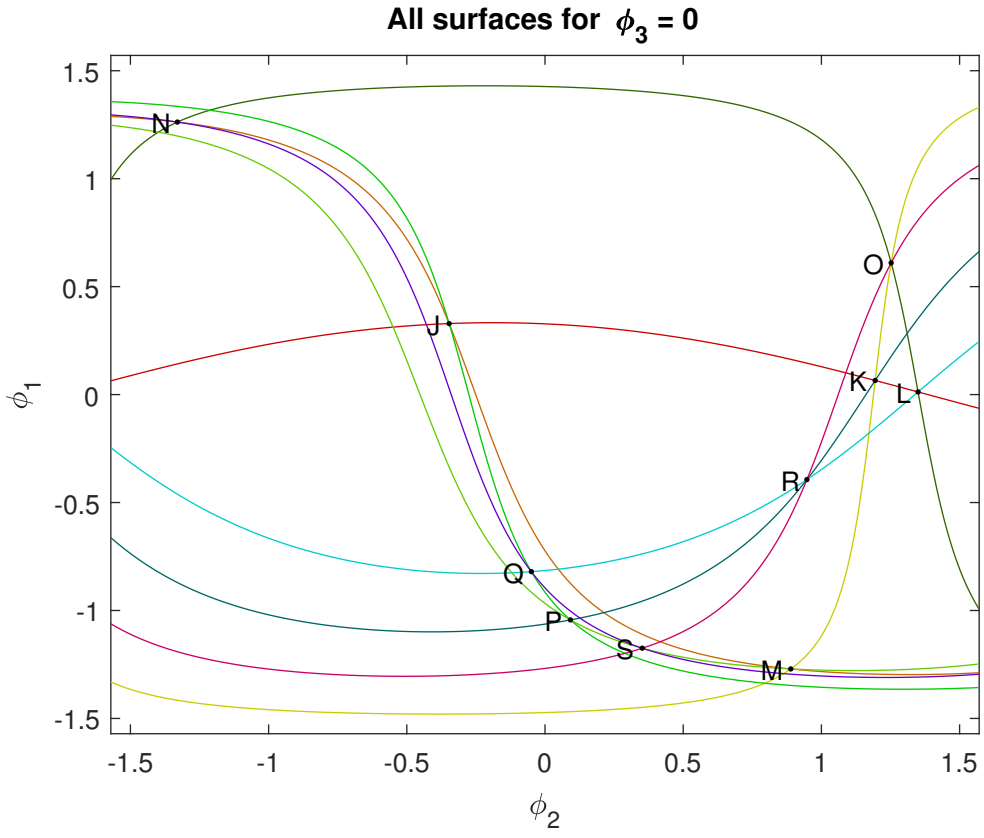

Figure 4.15: All surfaces for $\phi_3 = 0$.

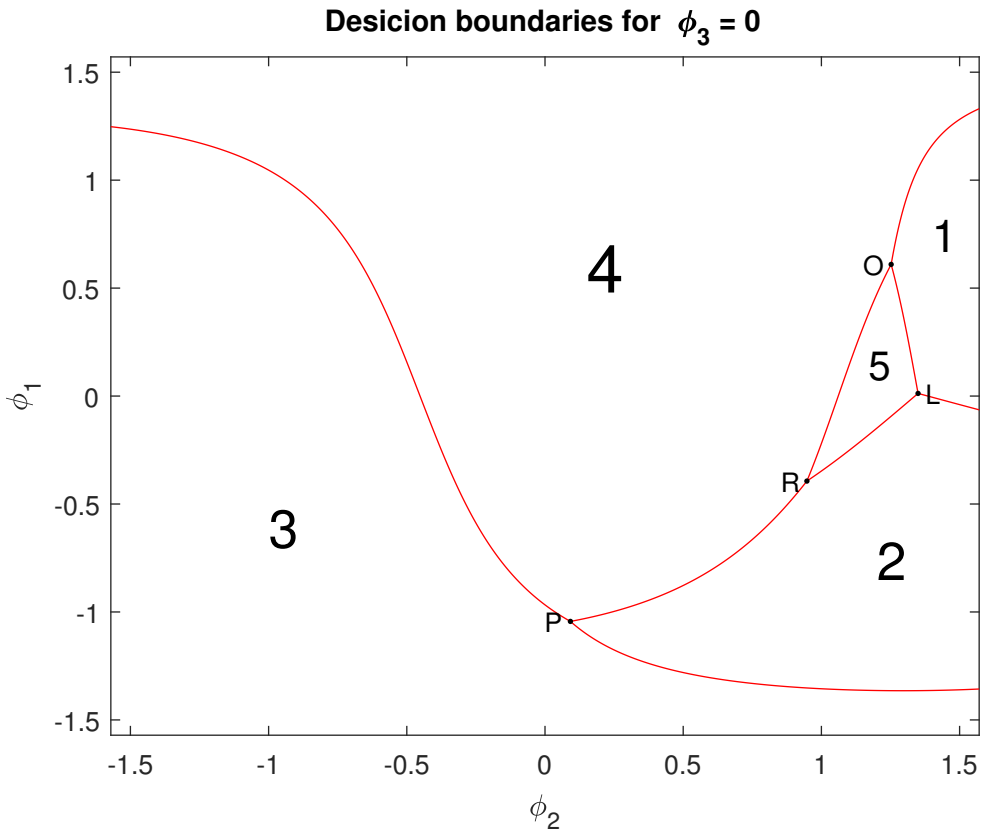

Figure 4.16: Decision boundaries for $\phi_3 = 0$.

Appendix

Appendix A

Since $\mathbf{C} = \sigma_n^2 \mathbf{I}_M$, the determinant $|\mathbf{C}|$ is the product of the diagonal units of $\mathbf{C}$ and is independent of x, which means that we can omit it from our maximization, having from (2.12) that

$$\boxed{\underset{x\in\mathcal{M}}{\operatorname{argmax}} f(\mathbf{r}|x) = \underset{x\in\mathcal{M}}{\operatorname{argmin}} (\mathbf{r}-\boldsymbol{\mu})^H \mathbf{C}^{-1} (\mathbf{r}-\boldsymbol{\mu})} \ . \tag{4.3}$$

Since $\boldsymbol{\mu} = \sqrt{P} h \mathbf{e}_x$ and $\mathbf{C}^{-1} = \frac{1}{\sigma_n^2}\mathbf{I}_M$, (4.3) becomes

$$\begin{aligned}
\underset{x\in\mathcal{M}}{\operatorname{argmax}} f(\mathbf{r}|x) &= \underset{x\in\mathcal{M}}{\operatorname{argmin}} \frac{1}{\sigma_n^2} (\mathbf{r} - \sqrt{P} h \mathbf{e}_x)^H \mathbf{I}_M (\mathbf{r} - \sqrt{P} h \mathbf{e}_x) \\
&= \underset{x\in\mathcal{M}}{\operatorname{argmin}} \mathbf{r}^H \mathbf{r} - \sqrt{P} h^* \mathbf{e}_x^T \mathbf{r} - \sqrt{P} h \mathbf{r}^H \mathbf{e}_x + P|h|^2 \mathbf{e}_x^T \mathbf{e}_x \\
&= \underset{x\in\mathcal{M}}{\operatorname{argmin}} \|\mathbf{r}\|^2 - \sqrt{P} h^* r_x - \sqrt{P} h r_x^* + P|h|^2 \\
&= \underset{x\in\mathcal{M}}{\operatorname{argmax}} \sqrt{P} h^* r_x + \sqrt{P} h r_x^* = \underset{x\in\mathcal{M}}{\operatorname{argmax}} 2\sqrt{P} \Re\{h^* r_x\} = \underset{x\in\mathcal{M}}{\operatorname{argmax}} \Re\{h^* r_x\} \ .
\end{aligned} \tag{4.4}$$

Appendix B

The covariance matrix is

$$\begin{aligned}
\mathbf{C} &= \mathbb{E}\big[\mathbf{r}\mathbf{r}^H | x\big] = \mathbb{E}\big[(\sqrt{P} h \mathbf{e}_x + \mathbf{n})(\sqrt{P} h \mathbf{e}_x + \mathbf{n})^H | x\big] \\
&= \mathbb{E}\big[P h h^* \mathbf{e}_x \mathbf{e}_x^T + \sqrt{P} h \mathbf{e}_x \mathbf{n}^H + \sqrt{P} h^* \mathbf{n} \mathbf{e}_x^T + \mathbf{n}\mathbf{n}^H\big] = P\sigma_h^2 \mathbf{e}_x \mathbf{e}_x^T + \sigma_n^2 \mathbf{I}_M \ .
\end{aligned} \tag{4.5}$$

From Matrix Determinant Lemma, we know that $|\mathbf{A}+\mathbf{u}\mathbf{u}^T| = (1+\mathbf{u}^T\mathbf{A}^{-1}\mathbf{u})|\mathbf{A}|$. Hence,

$$|\mathbf{C}| = |\sigma_n^2\mathbf{I}_M + (\sqrt{P}\sigma_h\mathbf{e}_x)(\sqrt{P}\sigma_h\mathbf{e}_x)^T| = \left(1+\sqrt{P}\sigma_h\mathbf{e}_x^T\frac{1}{\sigma_n^2}\mathbf{I}_M\sqrt{P}\sigma_h\mathbf{e}_x\right)|\sigma_n^2\mathbf{I}_M| = \left(1+P\frac{\sigma_h^2}{\sigma_n^2}\right)\sigma_n^{2M} .$$

We can see that the determinant $|\mathbf{C}|$ is independent of x and it can be omitted during the maximization of $f(\mathbf{r}|x)$, allowing us to use again (4.3) in maximizing our PDF.

Also, from Sherman-Morrison Formula, we know that $(\mathbf{A}+\mathbf{u}\mathbf{u}^H) = \mathbf{A}^{-1} - \frac{\mathbf{A}^{-1}\mathbf{u}\mathbf{u}^H\mathbf{A}^{-1}}{1+\mathbf{u}^H\mathbf{A}^{-1}\mathbf{u}}$. Hence,

$$\mathbf{C}^{-1} = \frac{1}{\sigma_n^2}\mathbf{I}_M - \frac{\frac{1}{\sigma_n^2}\mathbf{I}_M P\sigma_h^2\mathbf{e}_x\mathbf{e}_x^H\frac{1}{\sigma_n^2}\mathbf{I}_M}{1+\sqrt{P}\sigma_h\mathbf{e}_x^H\frac{1}{\sigma_n^2}\mathbf{I}_M\sqrt{P}\sigma_h\mathbf{e}_x} = \frac{1}{\sigma_n^2}\mathbf{I}_M - \frac{P\frac{\sigma_h^2}{\sigma_n^4}\mathbf{e}_x\mathbf{e}_x^H}{1+P\frac{\sigma_h^2}{\sigma_n^2}\mathbf{e}_x^H\mathbf{e}_x} = \frac{1}{\sigma_n^2}\mathbf{I}_M - \frac{P\sigma_h^2}{\sigma_n^2+P\sigma_h^2}\frac{1}{\sigma_n^2}\mathbf{e}_x\mathbf{e}_x^H$$

$$\Rightarrow \mathbf{C}^{-1} = \frac{1}{\sigma_n^2}\left(\mathbf{I}_M - \frac{P\sigma_h^2}{\sigma_n^2+P\sigma_h^2}\mathbf{e}_x\mathbf{e}_x^H\right) . \tag{4.6}$$

Then, from (4.3) we have that

$$\begin{aligned}\underset{x\in\mathcal{M}}{\operatorname{argmax}} f(\mathbf{r}|x) &= \underset{x\in\mathcal{M}}{\operatorname{argmin}}\,\mathbf{r}^H\mathbf{C}^{-1}\mathbf{r} = \underset{x\in\mathcal{M}}{\operatorname{argmin}}\,\frac{1}{\sigma_n^2}\left(\mathbf{r}^H\mathbf{r} - \frac{P\sigma_h^2}{\sigma_n^2+P\sigma_h^2}\mathbf{r}^H\mathbf{e}_x\mathbf{e}_x^H\mathbf{r}\right)\\ &= \underset{x\in\mathcal{M}}{\operatorname{argmin}} -\mathbf{r}^H\mathbf{e}_x(\mathbf{r}^H\mathbf{e}_x)^H = \underset{x\in\mathcal{M}}{\operatorname{argmax}}\, r_x^* r_x = \underset{x\in\mathcal{M}}{\operatorname{argmax}}\,|r_x|^2 = \underset{x\in\mathcal{M}}{\operatorname{argmax}}\,|r_x| .\end{aligned} \tag{4.7}$$

Appendix C

Since $\mathbf{C} = \sigma_w^2\mathbf{I}_{MN}$, the determinant $|\mathbf{C}|$ is the product of the diagonal units of $\mathbf{C}$ and is independent of $\mathbf{s}$, which means that we can omit it from our maximization, having from (2.22) that

$$\boxed{\underset{\mathbf{s}\in\mathcal{I}_M^N}{\operatorname{argmax}} f(\mathbf{y}|\mathbf{s}) = \underset{\mathbf{s}\in\mathcal{I}_M^N}{\operatorname{argmin}}(\mathbf{y}-\boldsymbol{\mu})^H\mathbf{C}^{-1}(\mathbf{y}-\boldsymbol{\mu})} . \tag{4.8}$$

Since $\boldsymbol{\mu} = \sqrt{P}h\mathbf{s}$ and $\mathbf{C}^{-1} = \frac{1}{\sigma_w^2}\mathbf{I}_{MN}$, (4.8) becomes

$$\begin{aligned}
\underset{\mathbf{s}\in\mathcal{I}_M^N}{\operatorname{argmax}} f(\mathbf{y}|\mathbf{s}) &= \underset{\mathbf{s}\in\mathcal{I}_M^N}{\operatorname{argmin}} \frac{1}{\sigma_w^2}(\mathbf{y}-\sqrt{P}h\mathbf{s})^H\mathbf{I}_{MN}(\mathbf{y}-\sqrt{P}h\mathbf{s}) \\
&= \underset{\mathbf{s}\in\mathcal{I}_M^N}{\operatorname{argmin}} \mathbf{y}^H\mathbf{y} - \sqrt{P}h\mathbf{y}^H\mathbf{s} - \sqrt{P}h^*\mathbf{s}^T\mathbf{y} + P|h|^2\mathbf{s}^T\mathbf{s} \\
&= \underset{\mathbf{s}\in\mathcal{I}_M^N}{\operatorname{argmin}} \|\mathbf{y}\|^2 - \sqrt{P}\big[(h^*\mathbf{s}^T\mathbf{y})^H + (h^*\mathbf{s}^T\mathbf{y})\big] + NP|h|^2 = \underset{\mathbf{s}\in\mathcal{I}_M^N}{\operatorname{argmax}} 2\Re\{h^*\mathbf{s}^T\mathbf{y}\} \\
&= \underset{\mathbf{s}\in\mathcal{I}_M^N}{\operatorname{argmax}} \Re\Big\{h^*\sum_{n=1}^{N}\mathbf{s}_{(n-1)M+1:nM,1}^T\mathbf{y}_{(n-1)M+1:nM,1}\Big\} \equiv \underset{\mathbf{x}\in\mathcal{M}^N}{\operatorname{argmax}} \sum_{n=1}^{N}\Re\{h^*y_n[x_n]\} \ .
\end{aligned} \tag{4.9}$$

Appendix D

The covariance matrix is

$$\begin{aligned}
\mathbf{C} &= \mathbb{E}[\mathbf{y}\mathbf{y}^H|\mathbf{s}] = \mathbb{E}[(\sqrt{P}h\mathbf{s}+\mathbf{w})(\sqrt{P}h\mathbf{s}+\mathbf{w})^H|\mathbf{s}] \\
&= \mathbb{E}[Phh^*\mathbf{s}\mathbf{s}^H + \sqrt{P}h\mathbf{s}\mathbf{w}^H + \mathbf{w}\sqrt{P}h^*\mathbf{s}^H + \mathbf{w}\mathbf{w}^H] = P\sigma_h^2\mathbf{s}\mathbf{s}^H + \sigma_w^2\mathbf{I}_{MN} \ .
\end{aligned} \tag{4.10}$$

Then, equivalently with the single symbol case, we have that

$$\begin{aligned}
\mathbf{C}^{-1} &= \frac{1}{\sigma_w^2}\mathbf{I}_{MN} - \frac{\frac{1}{\sigma_w^2}\mathbf{I}_{MN}P\sigma_h^2\mathbf{s}\mathbf{s}^H\frac{1}{\sigma_w^2}\mathbf{I}_{MN}}{1+\sqrt{P}\sigma_h\mathbf{s}^H\frac{1}{\sigma_w^2}\mathbf{I}_{MN}\sqrt{P}\sigma_h\mathbf{s}} \\
&= \frac{1}{\sigma_w^2}\mathbf{I}_{MN} - \frac{\frac{\sigma_h^2}{\sigma_w^4}P\mathbf{s}\mathbf{s}^H}{1+\frac{\sigma_h^2}{\sigma_w^2}NP} = \frac{1}{\sigma_w^2}\left(\mathbf{I}_{MN} - \frac{P\sigma_h^2}{\sigma_w^2+\sigma_h^2NP}\mathbf{s}\mathbf{s}^H\right) \ .
\end{aligned} \tag{4.11}$$

Hence, from (4.8) we have that

$$\begin{aligned}
\underset{\mathbf{s}\in\mathcal{I}_M^N}{\operatorname{argmax}} f(\mathbf{y}|\mathbf{s}) &= \underset{\mathbf{s}\in\mathcal{I}_M^N}{\operatorname{argmin}} \mathbf{y}^H\mathbf{C}^{-1}\mathbf{y} = \underset{\mathbf{s}\in\mathcal{I}_M^N}{\operatorname{argmin}} \frac{1}{\sigma_w^2}\left(\mathbf{y}^H\mathbf{y} - \frac{P\sigma_h^2}{\sigma_w^2+\sigma_h^2NP}\mathbf{y}^H\mathbf{s}\mathbf{s}^H\mathbf{y}\right) \\
&= \underset{\mathbf{s}\in\mathcal{I}_M^N}{\operatorname{argmax}} (\mathbf{y}^H\mathbf{s})(\mathbf{y}^H\mathbf{s})^H = \underset{\mathbf{s}\in\mathcal{I}_M^N}{\operatorname{argmax}} |\mathbf{y}^H\mathbf{s}|^2 \equiv \underset{\mathbf{x}\in\mathcal{M}^N}{\operatorname{argmax}} \left|\sum_{n=1}^{N} y_n[x_n]\right| \ .
\end{aligned} \tag{4.12}$$

Appendix E

$$\begin{aligned}
\max_{\mathbf{s}\in\mathcal{I}_M^N} f(\mathbf{Y}|\mathbf{s}) &\equiv \min_{\mathbf{s}\in\mathcal{I}_M^N} (\mathbf{z}-\boldsymbol{\mu})^H \mathbf{C}^{-1}(\mathbf{z}-\boldsymbol{\mu}) \equiv \min_{\mathbf{s}\in\mathcal{I}_M^N} \mathbf{z}^H\mathbf{z} - \mathbf{z}^H\boldsymbol{\mu} - \boldsymbol{\mu}^H\mathbf{z} + \boldsymbol{\mu}^H\boldsymbol{\mu} \\
&= \min_{\mathbf{s}\in\mathcal{I}_M^N} \|\mathbf{z}\|^2 - \mathbf{z}^H(\mathbf{h}\otimes\mathbf{s}) - (\mathbf{h}\otimes\mathbf{s})^H\mathbf{z} + (\mathbf{h}\otimes\mathbf{s})^H(\mathbf{h}\otimes\mathbf{s}) \\
&\equiv \max_{\mathbf{s}\in\mathcal{I}_M^N} \mathbf{z}^H(\mathbf{h}\otimes\mathbf{s}) + (\mathbf{h}\otimes\mathbf{s})^H\mathbf{z} + \mathbf{h}^H\mathbf{h}\otimes\mathbf{s}^H\mathbf{s} \\
&\equiv \max_{\mathbf{s}\in\mathcal{I}_M^N} \big((\mathbf{h}\otimes\mathbf{s})^H\mathbf{z}\big)^H + (\mathbf{h}\otimes\mathbf{s})^H\mathbf{z} = \max_{\mathbf{s}\in\mathcal{I}_M^N} 2\Re\{(\mathbf{h}\otimes\mathbf{s})^H\mathbf{z}\} \\
&\equiv \max_{\mathbf{s}\in\mathcal{I}_M^N} \Re\{(\mathbf{h}^H\otimes\mathbf{s}^H)\mathrm{vec}(\mathbf{Y})\} = \max_{\mathbf{s}\in\mathcal{I}_M^N} \Re\{\mathrm{vec}(\mathbf{s}^H\mathbf{Y}\mathbf{h}^*)\} \\
&\equiv \max_{\mathbf{s}_n\in\mathcal{I}_M} \sum_{n=1}^{N} \Re\{\mathbf{s}_n^T\mathbf{Y}_{n,:}\mathbf{h}^*\} \equiv \max_{\mathbf{x}\in\mathcal{M}^N} \sum_{n=1}^{N} \Re\{\mathbf{Y}_{n,:}[x_n]\mathbf{h}^*\}
\end{aligned}$$

$$\Rightarrow \boxed{\operatorname*{argmax}_{\mathbf{s}\in\mathcal{I}_M^N} f(\mathbf{Y}|\mathbf{s}) = \operatorname*{argmax}_{\mathbf{s}\in\mathcal{I}_M^N} \Re\{\mathbf{s}^H\mathbf{Y}\mathbf{h}^*\} \equiv \operatorname*{argmax}_{\mathbf{x}\in\mathcal{M}^N} \sum_{n=1}^{N} \Re\{\mathbf{Y}_{n,:}[x_n]\mathbf{h}^*\}} \tag{4.13}$$

Appendix F

The covariance matrix $\mathbf{C}$ can be determined as such

$$\begin{aligned}
\mathbf{C} &= \mathbb{E}[(\mathbf{z}-\boldsymbol{\mu})(\mathbf{z}-\boldsymbol{\mu})^H|\mathbf{s}] = \mathbb{E}[\mathbf{z}\mathbf{z}^H|\mathbf{s}] = \mathbb{E}[(\mathbf{h}\otimes\mathbf{s}+\mathbf{w})(\mathbf{h}\otimes\mathbf{s}+\mathbf{w})^H\ |\mathbf{s}] \\
&= \mathbb{E}[(\mathbf{h}\otimes\mathbf{s})(\mathbf{h}\otimes\mathbf{s})^H + (\mathbf{h}\otimes\mathbf{s})\mathbf{w}^H + \mathbf{w}(\mathbf{h}\otimes\mathbf{s})^H + \mathbf{w}\mathbf{w}^H\ |\mathbf{s}] = \mathbb{E}[\mathbf{h}\mathbf{h}^H\otimes\mathbf{s}\mathbf{s}^H\ |\mathbf{s}] + \sigma^2\mathbf{I}_{MND} \\
&= \sigma_h^2\mathbf{I}_D\otimes\mathbf{s}\mathbf{s}^H + \sigma^2\mathbf{I}_{MND} = \sigma_h^2\mathbf{I}_D^2\otimes\mathbf{s}\mathbf{s}^H + \sigma^2\mathbf{I}_{MND} = (\sigma_h\mathbf{I}_D\otimes\mathbf{s})(\sigma_h\mathbf{I}_D\otimes\mathbf{s})^H + \sigma^2\mathbf{I}_{MND} \\
&\Rightarrow \mathbf{C} = \mathbf{Q}\mathbf{Q}^H + \mathbf{A}, \text{ where } \mathbf{Q} = \sigma_h\mathbf{I}_D\otimes\mathbf{s} \text{ and } \mathbf{A} = \sigma^2\mathbf{I}_{MND}.
\end{aligned} \tag{4.14}$$

Using Woodbury's Identity we have that

$$\begin{aligned}
\mathbf{C}^{-1} &= (\mathbf{Q}\mathbf{Q}^H + \mathbf{A})^{-1} = (\mathbf{A} + \mathbf{Q}\mathbf{I}_D\mathbf{Q}^H)^{-1} = \mathbf{A}^{-1} - \mathbf{A}^{-1}\mathbf{Q}(\mathbf{I}_D + \mathbf{Q}^H\mathbf{A}^{-1}\mathbf{Q})^{-1}\mathbf{Q}^H\mathbf{A}^{-1} \\
&= \frac{1}{\sigma^2}\mathbf{I}_{MND} - \frac{1}{\sigma^2}\mathbf{I}_{MND}\mathbf{Q}(\mathbf{I}_D + \mathbf{Q}^H\frac{1}{\sigma^2}\mathbf{I}_{MND}\mathbf{Q})^{-1}\mathbf{Q}^H\frac{1}{\sigma^2}\mathbf{I}_{MND} \\
&\Rightarrow \mathbf{C}^{-1} = \frac{1}{\sigma^2}\Big[\mathbf{I}_{MND} - \frac{1}{\sigma^2}\mathbf{Q}(\mathbf{I}_D + \frac{1}{\sigma^2}\mathbf{Q}^H\mathbf{Q})^{-1}\mathbf{Q}^H\Big].
\end{aligned} \tag{4.15}$$

Also

$$\mathbf{s}^H\mathbf{s} = \begin{bmatrix}\mathbf{s}(1)^H & \dots & \mathbf{s}(N)^H\end{bmatrix}\begin{bmatrix}\mathbf{s}(1)\\ \vdots \\ \mathbf{s}(N)\end{bmatrix} = \mathbf{s}(1)^H\mathbf{s}(1) + \cdots + \mathbf{s}(N)^H\mathbf{s}(N) = N \tag{4.16}$$

and

$$\mathbf{Q}^H\mathbf{Q} = (\sigma_h\mathbf{I}\otimes\mathbf{s}^H)(\sigma_h\mathbf{I}\otimes\mathbf{s}) = \sigma_h^2\mathbf{I}_D\otimes\mathbf{s}^H\mathbf{s} = 2N\sigma_h^2\mathbf{I}_D. \tag{4.17}$$

Then, from (4.15) and (4.17) we have that

$$\begin{aligned}\mathbf{C}^{-1} &= \frac{1}{\sigma^2}\Big[\mathbf{I}_{MND} - \frac{1}{\sigma^2}\mathbf{Q}(\mathbf{I}_D + \frac{1}{\sigma^2}2N\sigma_h^2\mathbf{I}_D)^{-1}\mathbf{Q}^H\Big] = \frac{1}{\sigma^2}\Big[\mathbf{I}_{MND} - \frac{1}{\sigma^2}\mathbf{Q}\big[(1+\frac{1}{\sigma^2}2N\sigma_h^2)\mathbf{I}_D\big]^{-1}\mathbf{Q}^H\Big]\\ &= \frac{1}{\sigma^2}\Big[\mathbf{I}_{MND} - \frac{1}{\sigma^2}\frac{1}{(1+\frac{1}{\sigma^2}2N\sigma_h^2)}\mathbf{Q}\mathbf{I}_D\mathbf{Q}^H\Big]\\ &\Rightarrow \mathbf{C}^{-1} = \frac{1}{\sigma^2}\Big[\mathbf{I}_{MND} - \frac{1}{(\sigma^2+2N\sigma_h^2)}\mathbf{Q}\mathbf{Q}^H\Big]\ .\end{aligned} \tag{4.18}$$

For the determinant $|\mathbf{C}|$ we have that

$$\begin{aligned}|\mathbf{C}| &= |\mathbf{Q}\mathbf{Q}^H + \mathbf{A}| = |\mathbf{Q}\mathbf{Q}^H + \sigma^2\mathbf{I}_{MND}| = \sigma^{2MND}\Big|\frac{1}{\sigma^2}\mathbf{Q}\mathbf{Q}^H + \mathbf{I}_{MND}\Big|\\ &= \sigma^{2MND}\Big|\frac{1}{\sigma^2}\mathbf{Q}^H\mathbf{Q} + \mathbf{I}_{MND}\Big| = \sigma^{2MND}\Big|\frac{2N\sigma_h^2}{\sigma^2}\mathbf{I}_{MND} + \mathbf{I}_{MND}\Big|\\ &= \sigma^{2MND}\Big|\Big(\frac{2N\sigma_h^2}{\sigma^2}+1\Big)\mathbf{I}_{MND}\Big| = \sigma^{2MND}\Big(\frac{2N\sigma_h^2}{\sigma^2}+1\Big)^{MND}|\mathbf{I}_{MND}|\\ &\Rightarrow |\mathbf{C}| = (2N\sigma_h^2+\sigma^2)^{MND}.\end{aligned} \tag{4.19}$$

Appendix G

$$\begin{aligned}\max_{\mathbf{s}\in\mathcal{I}_M^N} f(\mathbf{Y}|\mathbf{s}) &\equiv \max_{\mathbf{s}\in\mathcal{I}_M^N} -\mathbf{z}^H\mathbf{C}^{-1}\mathbf{z} \equiv \min_{\mathbf{s}\in\mathcal{I}_M^N} -\mathbf{z}^H\mathbf{Q}\mathbf{Q}^H\mathbf{z} \equiv \max_{\mathbf{s}\in\mathcal{I}_M^N}(\mathbf{Q}^H\mathbf{z})^H(\mathbf{Q}^H\mathbf{z}) = \max_{\mathbf{s}\in\mathcal{I}_M^N}\|\mathbf{Q}^H\mathbf{z}\|^2\\ &\equiv \max_{\mathbf{s}\in\mathcal{I}_M^N}\|(\sigma_h\mathbf{I}_D\otimes\mathbf{s}^H)\mathbf{z}\| = \max_{\mathbf{s}\in\mathcal{I}_M^N}\|(\sigma_h\mathbf{I}_D\otimes\mathbf{s}^H)\mathrm{vec}(\mathbf{Y})\|\\ &= \max_{\mathbf{s}\in\mathcal{I}_M^N}\|\mathrm{vec}(\mathbf{s}^H\mathbf{Y}\sigma_h\mathbf{I}_D)\| \equiv \max_{\mathbf{s}\in\mathcal{I}_M^N}\|\mathrm{vec}(\mathbf{s}^H\mathbf{Y})\| \equiv \max_{\mathbf{s}\in\mathcal{I}_M^N}\|\mathbf{s}^H\mathbf{Y}\|\\ &\equiv \max_{\mathbf{s}_n\in\mathcal{I}_M}\sum_{n=1}^{N}\|\mathbf{s}_n^T\mathbf{Y}_{n,:}\| \equiv \max_{\mathbf{x}\in\mathcal{M}^N}\sum_{n=1}^{N}|\mathbf{Y}_{n,:}[x_n]|\\ &\Rightarrow \boxed{\operatorname*{argmax}_{\mathbf{s}\in\mathcal{I}_M^N} f(\mathbf{Y}|\mathbf{s}) = \operatorname*{argmax}_{\mathbf{s}\in\mathcal{I}_M^N}\|\mathbf{s}^H\mathbf{Y}\|}\end{aligned} \tag{4.20}$$

Appendix H

The decision for x_n will change from k to l (or vice versa), with $k, l \in \mathcal{M}$ and $k \neq l$ when

$$\Re\{\mathbf{Y}_{n,:}[k]\mathbf{c}(\boldsymbol{\phi})\} = \Re\{\mathbf{Y}_{n,:}[l]\mathbf{c}(\boldsymbol{\phi})\} \Leftrightarrow \Re\{(\mathbf{Y}_{n,:}[k] - \mathbf{Y}_{n,:}[l])\mathbf{c}(\boldsymbol{\phi})\} = 0$$

$$\Leftrightarrow \Re\left\{ (\mathbf{Y}_{n,:}[k] - \mathbf{Y}_{n,:}[l]) \begin{bmatrix} \cos\phi_1 \sin\phi_2 + j \sin\phi_1 \\ \cos\phi_1 \cos\phi_2 \cos\phi_3 + j \cos\phi_1 \cos\phi_2 \sin\phi_3 \end{bmatrix} \right\} = 0$$

$$\Leftrightarrow \Re\{\underbrace{(\mathbf{Y}_{n,1}[k] - \mathbf{Y}_{n,1}[l])}_{c_1}(\cos\phi_1 \sin\phi_2 + j \sin\phi_1)\} +$$

$$+ \Re\{\underbrace{(\mathbf{Y}_{n,2}[k] - \mathbf{Y}_{n,2}[l])}_{c_2} \cos\phi_1 \cos\phi_2 \cos\phi_3 + j \cos\phi_1 \cos\phi_2 \sin\phi_3\} = 0$$

$$\Leftrightarrow \Re\{c_1 \cos\phi_1 \sin\phi_2 + j c_1 \sin\phi_1 + c_2 \cos\phi_1 \cos\phi_2 \cos\phi_3 + j c_2 \cos\phi_1 \cos\phi_2 \sin\phi_3\} = 0$$

$$\Leftrightarrow \Re\{c_1\} \cos\phi_1 \sin\phi_2 - \Im\{c_1\} \sin\phi_1 + \Re\{c_2\} \cos\phi_1 \cos\phi_2 \cos\phi_3 - \Im\{c_2\} \cos\phi_1 \cos\phi_2 \sin\phi_3 = 0$$

$$\Leftrightarrow \begin{bmatrix} -\Im\{c_1\} & \Re\{c_1\} & -\Im\{c_2\} & \Re\{c_2\} \end{bmatrix} \begin{bmatrix} \sin\phi_1 \\ \cos\phi_1 \sin\phi_2 \\ \cos\phi_1 \cos\phi_2 \sin\phi_3 \\ \cos\phi_1 \cos\phi_2 \cos\phi_3 \end{bmatrix} = 0$$

$$\Leftrightarrow \boxed{\mathbf{y}_n^{\{k,l\}} \tilde{\mathbf{c}}(\boldsymbol{\phi}) = 0}$$

where

$$\mathbf{y}_n^{\{k,l\}} = \begin{bmatrix} \Im\{\mathbf{Y}_{n,1}[l] - \mathbf{Y}_{n,1}[k]\} \\ \Re\{\mathbf{Y}_{n,1}[k] - \mathbf{Y}_{n,1}[l]\} \\ \Im\{\mathbf{Y}_{n,2}[l] - \mathbf{Y}_{n,2}[k]\} \\ \Re\{\mathbf{Y}_{n,2}[k] - \mathbf{Y}_{n,2}[l]\} \end{bmatrix}.$$

Appendix I

For fixed ϕ_3, $k, l \in \mathcal{M}$ and $\phi_2 = -\frac{\pi}{2}$, we get from (3.9) that

$$\mathbf{y}^{\{k,l\}}\tilde{\mathbf{c}}(\boldsymbol{\phi}) = 0 \Leftrightarrow \begin{bmatrix} \Im\{\mathbf{Y}_{n,1}[l] - \mathbf{Y}_{n,1}[k]\} \\ \Re\{\mathbf{Y}_{n,1}[k] - \mathbf{Y}_{n,1}[l]\} \\ \Im\{\mathbf{Y}_{n,2}[l] - \mathbf{Y}_{n,2}[k]\} \\ \Re\{\mathbf{Y}_{n,2}[k] - \mathbf{Y}_{n,2}[l]\} \end{bmatrix}^T \begin{bmatrix} \sin\phi_1 \\ \cos\phi_1 \sin -\frac{\pi}{2} \\ \cos\phi_1 \cos -\frac{\pi}{2} \sin\phi_3 \\ \cos\phi_1 \cos -\frac{\pi}{2} \cos\phi_3 \end{bmatrix} = 0$$

$$\Leftrightarrow \; \Im\{\mathbf{Y}_{n,1}[l] - \mathbf{Y}_{n,1}[k]\} \sin\phi_1 - \Re\{\mathbf{Y}_{n,1}[k] - \mathbf{Y}_{n,1}[l]\} \cos\phi_1 = 0$$

$$\Leftrightarrow \boxed{\tan\phi_1 = \frac{\Re\{\mathbf{Y}_{n,1}[k] - \mathbf{Y}_{n,1}[l]\}}{\Im\{\mathbf{Y}_{n,1}[l] - \mathbf{Y}_{n,1}[k]\}}} \tag{4.21}$$

and for $\phi_2 = \frac{\pi}{2}$ that

$$\mathbf{y}^{\{k,l\}}\tilde{\mathbf{c}}(\boldsymbol{\phi}') = 0 \Leftrightarrow \begin{bmatrix} \Im\{\mathbf{Y}_{n,1}[l] - \mathbf{Y}_{n,1}[k]\} \\ \Re\{\mathbf{Y}_{n,1}[k] - \mathbf{Y}_{n,1}[l]\} \\ \Im\{\mathbf{Y}_{n,2}[l] - \mathbf{Y}_{n,2}[k]\} \\ \Re\{\mathbf{Y}_{n,2}[k] - \mathbf{Y}_{n,2}[l]\} \end{bmatrix}^T \begin{bmatrix} \sin\phi_1' \\ \cos\phi_1' \sin\frac{\pi}{2} \\ \cos\phi_1' \cos\frac{\pi}{2} \sin\phi_3 \\ \cos\phi_1' \cos\frac{\pi}{2} \cos\phi_3 \end{bmatrix} = 0$$

$$\Leftrightarrow \; \Im\{\mathbf{Y}_{n,1}[l] - \mathbf{Y}_{n,1}[k]\} \sin\phi_1' + \Re\{\mathbf{Y}_{n,1}[k] - \mathbf{Y}_{n,1}[l]\} \cos\phi_1' = 0$$

$$\Leftrightarrow \boxed{\tan\phi_1' = -\frac{\Re\{\mathbf{Y}_{n,1}[k] - \mathbf{Y}_{n,1}[l]\}}{\Im\{\mathbf{Y}_{n,1}[l] - \mathbf{Y}_{n,1}[k]\}}}\,. \tag{4.22}$$

Bibliography

[1] L. Freitag, M. Stojanovic, and M. Johnson, "Analysis of channel effects on direct-sequence and frequency-hopped spread-spectrum acoustic communication," *IEEE J. Ocean. Eng*, vol. 26, no. 4, pp. 586–593, Oct. 2001.

[2] F. Blackmon and L. Antonelli, "Remote, aerial, trans-layer, linear and non-linear downlink underwater acoustic communication," in *Proc. IEEE OCEANS 2006*, Boston, MA, Sep. 2006.

[3] R. Jurdak, P. Aguiar, P. Baldi, and C. V. Lopes, "Software modems for underwater sensor networks," in *Proc. IEEE OCEANS 2007*, Aberdeen, UK, Jun. 2007.

[4] Y. Li, X. Zhang, B. Benson, and R. Kastner, "Hardware implementation of symbol synchronization for underwater FSK," in *Proc. IEEE SUTC 2010*, Newport Beach, CA, Jun. 2010, pp. 82–88.

[5] Y. Li, B. Benson, R. Kastner, and L. Chen, "A new hardware design scheme of symbol synchronization for an underwater acoustic receiver," in *Third International Conference on Measuring Technology and Mechatronics Automation*, Shangshai, China, Jan. 2011, pp. 158–161.

[6] A. Sanchez, S. Blanc, P. Yuste, and J. J. Serrano, "A low cost and high efficient acoustic modem for underwater sensor networks," in *Proc. IEEE OCEANS 2011*, Santander, Spain, Jun. 2011.

[7] C. Petrioli, R. Petroccia, J. Shusta, and L. Freitag, "From underwater simulation to at-sea testing using the ns-2 network simulator," in *Proc. IEEE OCEANS 2011*, Santander, Spain, Jun. 2011.

[8] B. Zhang, Q. Zhan, S. Chen, M. Li, K. Ren, C. Wang, and D. Ma, "PriWhisper: Enabling keyless secure acoustic communication for smartphones," *IEEE Internet Things J.*, vol. 1, no. 1, pp. 33–45, Feb. 2014.

[9] S. Chen, M. Li, Z. Qin, B. Zhang, and K. Ren, "AcousAuth: An acoustic-based mobile application for user authentication," in *Proc. IEEE INFOCOM WKSHPS 2014*, Toronto, ON, May 2014, pp. 215–216.

[10] M. Kuba, M. Klatt, and A. Oeder, "Low-complexity sequence detection algorithm for FSK-based power line communications," in *Proc. IEEE ISPLC 2014,* Glasgow, UK, Apr. 2014, pp. 150–155.

[11] A. R. Ndjiongue, H. C. Ferreira, K. Ouahada, and A. J. Han Vinckz, "Low-complexity SOCPBFSK-OOK interface between PLC and VLC channels for low data rate transmission applications," in *Proc. IEEE ISPLC 2014,* Glasgow, UK, Apr. 2014, pp. 226–231.

[12] G. Vannucci, A. Bletsas, and D. Leigh, "A software-defined radio system for backscatter sensor networks," *IEEE Trans. Wireless Commun.*, vol. 7, no. 6, pp. 2170–2179, Jun. 2008.

[13] J. Kimionis, A. Bletsas, and J. N. Sahalos, "Increased range bistatic scatter radio," *IEEE Trans. Commun.*, vol. 62, no. 3, pp. 1091–1104, Mar. 2014.

[14] P. N. Alevizos, N. Fasarakis-Hilliard, K. Tountas, N. Agadakos, N. Kargas, and A. Bletsas, "Channel coding for increased range bistatic backscatter radio: Experimental results," in *Proc. IEEE RFID-TA 2014*, Tampere, Finland, Sep. 2014.

[15] N. Fasarakis-Hilliard, P. N. Alevizos, and A. Bletsas, "Coherent detection and channel coding for bistatic scatter radio sensor networking," *IEEE Trans. Commun.* vol. 63, no. 5, pp. 1798–1810, May 2015.

[16] P. N. Alevizos and A. Bletsas, "Noncoherent composite hypothesis testing receivers for extended range bistatic scatter radio WSNs," in *Proc. IEEE ICC 2015*, London, UK, Jun. 2015, pp. 4448–4453.

[17] H. Okada and T. Itoh, "M-ary FSK modulation using short packet without a preamble and error detection codes for low power wireless communication," *Wireless Sensor Network*, vol. 6, pp. 35–42, 2014.

[18] R. Annavajjala, P. C. Cosman, and L. B. Milstein, "On the performance of optimum noncoherent amplify-and-forward reception for cooperative diversity," in *Proc. IEEE MILCOM 2005*, Atlantic City, NJ, Oct. 2005, pp. 3280–3288.

[19] D. Chen and J. N. Laneman, "Modulation and demodulation for cooperative diversity in wireless systems," *IEEE Trans. Wireless Commun.*, vol. 5, no. 7, pp. 1785–1794, Jul. 2006.

[20] M. R. Souryal, "Non-coherent amplify-and-forward generalized likelihood ratio test receiver," *IEEE Trans. Wireless Commun.*, vol. 9, no. 7, pp. 2320–2327, Jul. 2010.

[21] G. Farhadi and N. C. Beaulieu, "A low complexity receiver for noncoherent amplify-and-forward cooperative systems," *IEEE Trans. Commun.*, vol. 58, no. 9, pp. 2499–2504, Sep. 2010.

[22] H. X. Nguyen, H. H. Nguyen, and T. Le-Ngoc, "Noncoherent receiver for amplify-and-forward relaying with M-FSK modulation," in *Proc. IEEE GLOBECOM 2011*, Houston, TX, Dec. 2011.

[23] P. Liu, S. Gazor, I.-M. Kim, and D. I. Kim, "Noncoherent amplify-and-forward cooperative networks: Robust detection and performance analysis," *IEEE Trans. Commun.*, vol. 61, no. 9, pp. 3644–3659, Jun. 2013.

[24] Y. Iwanami and P. H. Wittke, "Error performance analysis of an energy sequence estimation receiver for binary FSK on frequency-selective fading channels," *IEEE Trans. Wireless Commun.*, vol. 2, no. 2, pp. 260–269, Mar. 2003.

[25] I. Korn, J. P. Fonseka, and S. Xing, "Optimal binary communication with nonequal probabilities," *IEEE Trans. Commun.*, vol. 51, no. 9, pp. 1435–1438, Sep. 2003.

[26] S. Sharma, G. Yadav, and A. K. Chaturvedi, "Multicarrier on-off keying for fast frequency hopping multiple access systems in Rayleigh fading channels," *IEEE Trans. Wireless Commun.*, vol. 6, no. 3, pp. 769–774, Mar. 2007.

[27] M. C. Gursoy, "Error rate analysis for peaky signaling over fading channels," *IEEE Trans. Commun.*, vol. 57, no. 9, pp. 2546–2550, Sep. 2009.

[28] J. G. Proakis and M. Salehi, *Digital Communications*, 5th Ed. Upper Saddle River, NJ: Prentice-Hall, Nov. 2007.

[29] D. Warrier and U. Madhow, "Spectrally efficient noncoherent communication," *IEEE Trans. Inf. Theory,* vol. 48, no. 3, pp. 651–668, Mar. 2002.

[30] R.-R. Chen, R. Koetter, U. Madhow, and D. Agrawal, "Joint noncoherent demodulation and decoding for the block fading channel: A practical framework for approaching Shannon capacity," *IEEE Trans. Commun.*, vol. 51, no. 10, pp. 1676–1689, Oct. 2003.

[31] D. Makrakis and P. T. Mathiopoulos, "Optimal decoding in fading channels: A combined envelope, multiple differential and coherent detection approach," *in Proc. IEEE GLOBECOM 1989*, Dallas, TX, Nov. 1989, vol. 3, pp. 1551–1557.

[32] S. G. Wilson, J. Freebersyser, and C. Marshall, "Multi-symbol detection of M-DPSK," *in Proc. IEEE GLOBECOM 1989*, Dallas, TX, Nov. 1989, vol. 3, pp. 1692–1697.

[33] D. Divsalar and M. K. Simon, "Multiple-symbol differential detection of MPSK," *IEEE Trans. Commun.*, vol. 38, no. 3, pp. 300–308, Mar. 1990.

[34] H. Leib and S. Pasupathy, "Noncoherent block demodulation of PSK," in *Proc. IEEE VTC 1990*, Orlando, FL, May 1990, pp. 407–411.

[35] C.-D. Chung and F.-C. Hung, "Noncoherent maximum-likelihood block detection of orthogonal NFSK-LDPSK signals," *IEEE Trans. Vehic. Tech.*, vol. 51, no. 2, pp. 283–292, Mar. 2002.

[36] C.-D. Chung, "Coherent and differentially coherent detections of orthogonally multiplexed orthogonal phase-modulated signals," *IEEE Trans. Commun.*, vol. 51, no. 3, pp. 428–440, Mar. 2003.

[37] K. Mackenthun, "A fast algorithm for maximum likelihood detection of QPSK or $\pi/4$-QPSK sequences with unknown phase," in *Proc. IEEE PIMRC 1992*, Boston, MA, Oct. 1992, pp. 240–244.

[38] K. M. Mackenthun, Jr., "A fast algorithm for multiple-symbol differential detection of MPSK," *IEEE Trans. Commun.*, vol. 42, pp. 1471–1474, Feb./Mar./Apr. 1994.

[39] G. N. Karystinos and D. A. Pados, "Rank-2-optimal adaptive design of binary spreading codes," *IEEE Trans. Inf. Theory*, vol. 53, no. 9, pp. 3075–3080, Sep. 2007.

[40] D. S. Papailiopoulos, G. A. Elkheir, and G. N. Karystinos, "Maximum-likelihood noncoherent PAM detection," *IEEE Trans. Commun.*, vol. 61, no. 3, pp. 1152–1159, Mar. 2013.

[41] W. Sweldens, "Fast block noncoherent decoding," *IEEE Commun. Letters,* vol. 5, no. 4, pp. 132–134, Apr. 2001.

[42] I. Motedayen-Aval, A. Krishnamoorthy, and A. Anastasopoulos, "Optimal joint detection/estimation in fading channels with polynomial complexity," *IEEE Trans. Inf. Theory,* vol. 53, no. 1, pp. 209–223, Jan. 2007.

[43] I. Motedayen-Aval and A. Anastasopoulos, "Polynomial-complexity noncoherent symbol-by-symbol detection with application to adaptive iterative decoding of turbo-like codes," *IEEE Trans. Commun.*, vol. 51, no. 2, pp. 197–207, Feb. 2003.

[44] D. J. Ryan, I. B. Collings, and I. V. L. Clarkson, "GLRT-optimal noncoherent lattice decoding," *IEEE Trans. Signal. Proc.*, vol. 55, no. 7, pp. 3773–3786, Jul. 2007.

[45] R. G. McKilliam, D. J. Ryan, I. V. L. Clarkson, and I. B. Collings, "An improved algorithm for optimal noncoherent QAM detection," in *Proc. 2008 Australian Commun. Theory Workshop*, Christchurch, New Zealand, Feb. 2008, pp. 64–68.

[46] M. Simon and D. Divsalar, "Some interesting observations for certain line codes with application to RFID," *IEEE Trans. Commun.*, vol. 54, no. 4, pp. 583–586, Apr. 2006.

[47] C. Angerer, "Design and exploration of radio frequency identification systems by rapid prototyping," Ph.D. dissertation, Vienna University of Technology, Jul. 2010.

[48] M. Mohaisen, H. Yoon, and K. Chang, "Radio transmission performance of EPCglobal Gen-2 RFID system," in *Proc. IEEE ICACT 2008*, Gangwon-Do, South Korea, Dec. 2008, pp. 1423–1428.

[49] S. M. Yeo, B. Jeon, J. H. Bae, Y. J. Moon, Y. J. Kim, H. H. Roh, J. S. Park, Y. R. Seong, H. R. Oh, J. S. Kim, C. W. Park, and G. Y. Choi, "A channel allocation scheme considering

with collisions and interferences in practical UHF RFID applied communication fields," in *Proc. IEEE RFID 2008*, Las Vegas, NV, Apr. 2008, pp. 258–268.

[50] R. Hoefel and D. Franco, "Joint performance and link budget analysis of HF RFID technology over fast and block fading channels," in *Proc. IEEE ICT 2009*, Marrakech, Morocco, May 2009, pp. 103–108.

[51] A. Lazaro, D. Girbau, and R. Villarino, "Effects of interferences in UHF RFID systems," *Progress In Electromagnetics Research*, vol. 98, pp. 425–443, 2009.

[52] C. Angerer, R. Langwieser, and M. Rupp, "RFID reader receivers for physical layer collision recovery," *IEEE Trans. Commun.*, vol. 58, no. 12, pp. 3526–3537, Dec. 2010.

[53] S. Thomas and M. S. Reynolds, "QAM backscatter for passive UHF RFID tags," in *Proc. IEEE RFID 2010*, Orlando, FL, Apr. 2010, pp. 210–214.

[54] Y. Yuan and D. Yu, "Reader planning in UHF RFID application," in *Proc. IEEE RFID-TA 2011*, Sitges, Spain, Sep. 2011, pp. 272–278.

[55] R. Morelos-Zaragoza, "On error performance improvements of passive UHF RFID systems via syndrome decoding," in *Proc. IEEE iThings/CPSCom 2011*, Dalian, China, Oct. 2011, pp. 127–130.

[56] J. Park and T.-J. Lee, "Channel-aware line code decision in RFID," *IEEE Commun. Lett.*, vol. 15, no. 12, pp. 1402–1404, Dec. 2011.

[57] A. Bletsas, J. Kimionis, A. G. Dimitriou, and G. N. Karystinos, "Single antenna coherent detection of collided FM0 RFID signals," *IEEE Trans. Commun.*, vol. 60, no. 3, pp. 756–766, Mar. 2012.

[58] R. Morelos-Zaragoza, "Unequal error protection with CRC-16 bits in EPC class-1 generation-2 UHF RFID systems," in *Proc. IEEE ISITA 2012*, Honolulu, HI, Oct. 2012, pp. 36–40.

[59] J. Park, J. Lee, H. Han, and T.-J. Lee, "Adaptive line code selection by identification efficiency for RFID systems," in *Proc. ACM ICUIMC 2012*, Kuala Lumpur, Malaysia, Feb. 2012, pp. 1–4.

[60] S.-B. Yim, J. Park, and T.-J. Lee, "Novel dynamic framed-slotted ALOHA using litmus slots in RFID systems," in *IEICE Trans. Commun.*, vol. E95-B, no. 4, pp. 1375–1383, Apr. 2012.

[61] S.-Y. Ahn, J.-S. Park, Y. R. Seong, and H.-R. Oh, "Performance evaluation of mobile RFID under multiple BoMR environments," in *Proc. IEEE ICUFN 2012*, Phuket, Thailand, Jul. 2012, pp. 484–489.

[62] Y. Yuan and D. Yu, "Nested error correcting code based highly reliable data reading for UHF RFID," in *Proc. IEEE RFID 2013*, Penang, Malaysia, May 2013, pp. 160–167.

[63] A. Schantin, "Iterative decoding of baseband and channel codes in a long-range RFID system," in *Proc. IEEE ICIT 2013*, Cape Town, South Africa, Feb. 2013, pp. 1671–1676.

[64] A. Schantin and C. Ruland, "Retransmission strategies for RFID systems using the EPC protocol," in *Proc. IEEE RFID-TA 2013*, Johor Bahru, Malaysia, Sep. 2013, pp. 1–6.

[65] J. G. Goh and S. V. Marić, "The capacities of frequency-hopped code-division multiple-access channels," *IEEE Trans. Inf. Theory,* vol. 44, no. 3, pp. 1204–1211, May 1998.

[66] C.-D. Chung, "Differential detection of quadrature frequency/phase modulated signals," *IEEE Trans. Commun.*, vol. 47, no. 4, pp. 546–557, Apr. 1999.

[67] S. H. Kim and S. W. Kim, "Frequency-hopped multiple-access communications with multicarrier on-off keying in Rayleigh fading channels," *IEEE Trans. Commun.,* vol. 48, no. 10, pp. 1692–1701, Oct. 2000.

[68] C. D. Meyer, *Matrix Analysis and Applied Linear Algebra.* Philadelphia, PA: SIAM, 2000.

[69] S. Gazor, M. Derakhtian, and A. A. Tadaion, "Computationally efficient maximum likelihood sequence estimation and activity detection for M-PSK signals in unknown flat fading channels," *IEEE Signal Process. Lett.,* vol. 17, no. 10, pp. 871–874, Oct. 2010.

[70] R. G. McKilliam, A. Pollok, B. Cowley, I. V. L. Clarkson, and B. G. Quinn, "Noncoherent least squares estimators of carrier phase and amplitude," in *Proc. IEEE ICASSP 2013*, Vancouver, BC, May 2013, pp. 4888–4892.

[71] P. N. Alevizos, Y. Fountzoulas, G.N. Karystinos, and A. Bletsas, "Log-Linear-Complexity GLRT-Optimal Noncoherent Sequence Detection fo Orthogonal and RFID-Oriented Modulations," in *IEEE Trans. Commun.*, vol. 64, no. 4, April 2016, pp. 1600–1612.